EUROPEAN ORGANIZATION FOR NUCLEAR RESEARCH

L3 Note 2561
July 4, 2000

Moments of the charged-particle multiplicity distribution in Z decays at LEP

The L3 collaboration

Abstract

Preliminary results are presented on the charged-particle multiplicity distribution and inclusive particle momentum spectrum in e^+e^- collisions at the Z mass. The charged-particle multiplicity distribution, its mean and higher moments have been measured, for all hadronic as well as for light-quark and b-quark events. The H_q moments derived from the charged-particle multiplicity distribution are known to exhibit quasi-oscillations when plotted versus the order of the moment. This behavior is predicted by the NNLLA of perturbative QCD for the parton level and, under the assumption of LPHD, also for the hadron level. Such quasi-oscillations are also seen in our data. Using the jet multiplicity distributions, obtained from the Cambridge jet algorithm, in order to vary the dependence on the LPHD hypothesis, we find, however, that at our energy the oscillations only appear for non-perturbative scales. Since the weak b-decay is known to distort the multiplicity distribution and since NNLLA is based on massless quarks, the analysis is repeated for both tagged light-quark and b-quark samples.

Submitted to the *XXXth International Conference on High Energy Physics*
July 27 - August 2, 2000, Osaka, Japan

Introduction

Although the number of charged particles (the charged-particle multiplicity n) is only a global measure of the characteristics of the final state of a high-energy collision, it has proved a fundamental tool in the study of particle production. Independent emission of single particles leads to a Poissonian multiplicity distribution. Deviations from this shape, therefore, reveal correlations [1].

The shape of a distribution can be described in terms of its moments of all orders. Normalized factorial moments of order q are defined in terms of the multiplicity distribution, P_n, by

$$F_q = \frac{\sum_{n=q}^{\infty} n(n-1)....(n-q+1)P_n}{\left(\sum_{n=1}^{\infty} nP_n\right)^q} \quad .$$

The factorial moment of order q corresponds to an integral over the q-particle density and reflects correlations in particle production. If particles are produced independently the particle distribution is Poissonian, for which all F_q are equal to one. If the particles are correlated, the distribution is broader than Poisson and the F_q are greater than one. If the particles are anti-correlated, the distribution is narrower than Poisson and the F_q are smaller than one.

The normalized cumulant factorial moments are obtained from the normalized factorial moments by

$$K_q = F_q - \sum_{m=0}^{q-1} \frac{(q-1)!}{m!(q-m-1)!} K_{q-m} F_m \ .$$

The cumulant factorial moment, K_q, corresponds to the phase-space integral over the q-particle correlation function which describes the genuine correlations between q particles.

Since $|K_q|$ and F_q increase rapidly with their moment order, it is useful to define the ratio $H_q = \frac{K_q}{F_q}$, which has the same order of magnitude over a large range of q. One can view this ratio as a cumulant factorial moment normalized to the factorial moment. It reflects the genuine q-particle correlation integral relative to the density integral. The behavior of F_q and H_q with moment order q is shown in fig. 1 for the Poisson distribution and for the negative binomial distribution which is often used to fit the charged-particle multiplicity distribution [2].

The H_q have been calculated for the soft gluon multiplicity distribution for different approximations of perturbative QCD (pQCD) [3]. The behavior of the H_q with moment order q appeared to be dependent of the approximation used:

- For the Double Leading Logarithm Approximation (DLLA), H_q decreases to 0 as q^{-2}.
- For the Modified Leading Logarithm Approximation (MLLA), H_q decreases to a negative minimum at $q = 5$, and then rises to approach 0 asymptotically.
- For the Next to Leading Logarithm Approximation (NLLA), H_q decreases to a positive minimum at $q = 5$ and then increases to a positive constant value for large moment rank.
- For the Next to Next to Leading Logarithm Approximation (NNLLA), H_q decreases to a negative first minimum for $q = 5$ and shows quasi-oscillations about 0 for $q > 5$.

These behaviors are illustrated in figure 2. Assuming the validity of the Local Parton Hadron Duality hypothesis (LPHD), such behavior is also expected for the charged-particle multiplicity distribution.

The H_q of the charged-particle multiplicity distribution have been measured by the SLD collaboration [4] for $e^+e^- \longrightarrow$ hadrons at $\sqrt{s} = M_Z$. They observed a negative minimum for $q = 5$ followed by quasi-oscillations about 0 for higher q. This result has indeed been interpreted as a confirmation of the NNLLA prediction.

The H_q moments have also been calculated [5,6] from published charged-particle multiplicity distributions of ALEPH [7], DELPHI [8], OPAL [9] and in each case, similar behavior with a negative first minimum followed by quasi-oscillation about 0 has been seen. Furthermore, this result is not limited to e^+e^- physics; the oscillatory behavior of the H_q moments has also been observed in hadronic collisions [10] between 20 and 900 GeV.

While it is tempting to conclude that the observed behavior is a confirmation of the NNLLA prediction, it must be realized that such a conclusion rests strongly on the validity of the LPHD hypothesis. The LPHD asserts that the shape of the parton distribution is not altered by the hadronization phase, therefore particle and parton distributions differ only by a change of scale. Although this hypothesis is accepted for single-particle distributions and the energy dependence of the mean multiplicity, difficulties have been detected when resonances are involved [11, 12]. Further, heavy quark decays will cause a modification of the multiplicity distribution which is unlikely to be properly accounted for by LPHD [6]. For these reasons, we consider the assumption of LPHD as highly questionable.

Therefore, in this paper we present preliminary measurements of the ratio of cumulant to factorial moments not only of the charged-particle multiplicity distribution for all hadronic events, but also for tagged light-quark events. This, in order to comply with the theoretical framework and for a better reliability with pQCD calculations, which usually assume massless quarks. In order to check the influence of heavy-quark decay on the charged-particle multiplicity distribution, the analysis is also performed on tagged b-quark events.

We further extend the analysis to the study of the jet multiplicity distributions obtained for various values of the jet resolution parameter. By varying this parameter (and hence the energy scale), we can, in some sense, follow the development of partons to hadrons. The variation of the mean jet multiplicity with the jet resolution parameter has been found [13–16] to agree well with analytic NLLA QCD calculations in the perturbative region (energy scale greater than about $1 - 2$ GeV) and with Monte Carlo models in both the perturbative and the non-perturbative region. These jet multiplicity distributions should, therefore, enable us to extend the moment-ratio analysis to the energy scales of partons and to that of perturbative QCD, avoiding (or at least reducing) the dependence on the LPHD assumption.

Selection and correction procedures on the data

This analysis is based on data collected by the L3 detector [17] in 1994 and 1995 at the energy of the Z. The data sample corresponds to approximately 1.5 million produced hadronic Z decays.

Events are selected in a two-step procedure, which begins with a pre-selection using the energy measured in the electro-magnetic and hadronic calorimeters. All calorimeter clusters are required to have an energy of at least 100 MeV. Hadronic events are then selected by requiring

$$0.5 < \frac{E^{\rm cal}}{\sqrt{s}} < 1.5 \ , \ \frac{|E_{\parallel}^{\rm cal}|}{E^{\rm cal}} < 0.4 \ \text{and} \ \frac{|E_{\perp}^{\rm cal}|}{E^{\rm cal}} < 0.6 \quad ,$$

where $E^{\rm cal}$ is the total calorimeter energy, $E_{\parallel}^{\rm cal}$ is the energy imbalance along the beam direction and $E_{\perp}^{\rm cal}$ is the energy imbalance in the plane perpendicular to the beam direction. To ensure that the event fully lies within the acceptance of the calorimeter, selected events are required to have $|\cos(\theta_{\rm th}^{\rm cal})| \leq 0.74$, where $\theta_{\rm th}^{\rm cal}$ is the polar angle of the event thrust axis determined from calorimeter clusters. Furthermore at least 15 clusters are required, in order to reduce background from $\rm e^+e^- \longrightarrow \tau^+\tau^-$.

The advantage of the pre-selection is that it largely decouples the event selection from the track selection, allowing relatively weak cuts on track momenta. This reduces systematic errors in the charged-particle multiplicity distribution on which our analysis is based.

The second step of the procedure is the selection of charged tracks from events which have passed the pre-selection. It is based on the track momenta measured in the Central Tracking Detector including the Silicon Micro-vertex Detector. A number of quality cuts are defined to select well-measured tracks. Hadronic events are then selected by requiring a thrust-axis direction within $|\cos(\theta_{\rm th}^{\rm TEC})| \leq 0.7$, where $\theta_{\rm th}^{\rm TEC}$ is the polar angle of the event thrust axis determined from the momenta $\vec{p}$ of well-measured charged tracks. About 990000 events survive this selection.

The multiplicity distributions obtained from the raw data were corrected for detector acceptance and efficiency and for the selection procedure by the following method. Events are generated by the Monte Carlo programs JETSET 7.4 PS [18] and ARIADNE 4.2 [19], which have been tuned using L3 data [21]. For each MC sample, a multiplicity distribution, $P^{\rm gen}(n_{\rm gen})$, is first determined at the generator level. The events are then passed through the simulation of the L3 detector [22] and reconstructed using the same program as is used for the data. After the above-described event- and track-selection procedure a multiplicity distribution, $P_n^{\rm det}$, is obtained at the detector level. The probability matrix $M(n_{\rm det}, n_{\rm gen})$, representing the probability to obtain an event with $n_{\rm det}$ detector-level tracks from $n_{\rm gen}$ generated particles, is built. It takes into account the migration of the number of tracks between the generator and detector level due to detector limitations. This matrix is the main component of the unfolding method [23] used here. This unfolding method uses an iterative procedure to correct the data and has the advantage over the commonly used matrix inversion method of being less Monte Carlo dependent.

The unfolding starts by comparing the multiplicity distribution of the raw data to the detector-level Monte Carlo using the ratio:

$$C_{\rm det}^1(n_{\rm det}) = \frac{P^{\rm raw}(n_{\rm det})}{P^{\rm det}(n_{\rm det})}, \text{ where } P^{\rm det}(n_{\rm det}) = \sum_{n_{\rm gen}} M(n_{\rm det}, n_{\rm gen}) \times P^{\rm gen}(n_{\rm gen}).$$

The χ^2 between $P^{\rm raw}(n_{\rm det})$ and $\sum\limits_{n_{\rm gen}} M(n_{\rm det}, n_{\rm gen}) \times P^{\rm gen}(n_{\rm gen})$ is also calculated.

The $C_{\rm det}^1$ correction factors are passed through the matrix $D(n_{\rm gen}, n_{\rm det})$, the transpose of the matrix $M(n_{\rm det}, n_{\rm gen})$ to lead to a set of correction factors at generator level $C_{\rm gen}^1(n_{\rm gen}) = \sum\limits_{n_{\rm det}} D(n_{\rm gen}, n_{\rm det}) \times C_{\rm det}^1(n_{\rm det})$.

The $C_{\rm gen}^1$ correction factors are then applied to the Monte Carlo multiplicity distribution at generator level to obtain a new multiplicity $P^1(n_{\rm gen}) = P^{\rm gen}(n_{\rm gen}) \times C_{\rm gen}^1(n_{\rm gen})$

This new multiplicity distribution $P^1(n_{\rm gen})$ represents the estimate of the corrected data multiplicity distribution for the first iteration. Depending on the value of the χ^2 between $P^{\rm raw}(n_{\rm det})$ and $\sum M(n_{\rm det}, n_{\rm gen}) \times P^1(n_{\rm gen})$, the procedure is repeated with P^1 instead of $P^{\rm gen}$ and leads to $P^2(n_{\rm gen}) = P^1(n_{\rm gen}) \times C^2_{\rm gen}(n_{\rm gen})$. The iterative process is repeated until the χ^2/dof becomes small enough (e.g. order of 1). In our analysis, multiplicity distributions obtained after the second iteration, were used as reconstructed multiplicity distributions (the χ^2 were smaller than one)

Two additional corrections were applied to the data in order to get the fully reconstructed multiplicity distribution.

1. To correct the data for Initial State Radiation, two Monte Carlo samples with and without ISR were generated and the reconstructed data were multiplied by the ratio $P^{\rm noISR}_{\rm gen}/P^{\rm ISR}_{\rm gen}$.

2. In order to be able to compare to other e^+e^- experiments, the data were further corrected to reintroduce the charged K^0_s and Λ decay products. It must be noted that the K^0_s and Λ have decayed at detector level, while they remain undecayed at generator level (therefore, by correction for detector acceptance and efficiency, the K^0_s and Λ decay products are removed). In order to add the charged K^0_s and Λ decay products, we built, using the JETSET 7.4 PS generator, a matrix $K(n_{\rm K^0}, n_{\rm noK^0})$ representing the number of events with $n_{\rm K^0}$ particles in the case that K^0_s and Λ have decayed and $n_{\rm noK^0}$ particles in the case that K^0_s and Λ remain stable. The Charged-particle multiplicity distribution including K^0_s and Λ decay products is then given by $P^{\rm K^0}_{\rm data}(n_{\rm K^0}) = \sum (K(n_{\rm K^0}, n_{\rm noK^0})/P^{\rm noK^0}_{\rm MC}(n_{\rm noK^0})) \times P_{\rm data}(n_{\rm noK^0})$.

Statistical and systematic errors

The statistical errors of the moments (both basic moments and H_q) are found by propagating the errors on the corrected multiplicity distribution using the full covariance matrix which takes into account all the corrections applied to the data (i.e. unfolding procedure and bin by bin corrections terms). Multinomial errors are assumed for all distributions.

Systematic errors were estimated from three different sources:

1. The influence of the model used to correct the data, by using ARIADNE instead of JETSET.

2. The influence of the unfolding method. This was investigated by comparing the generator level distribution of JETSET to that obtained by unfolding the detector level of JETSET using a matrix determined using ARIADNE, and by a similar comparison where the roles OF JETSET and ARIADNE were exchanged.

3. The influence of the selection procedure, obtained by varying independently the cuts used in the selection procedure and by changing the track quality cuts (which give the largest important contribution to the systematics errors).

   In addition for the selection of light- or b-quark, we checked the influence of the purity and efficiency in light- or b-quark by varying the cut on the discriminant value of the tagging (described below).

All systematic uncertainties and statistical errors were added in quadrature. Other sources of systematic errors are still under investigation. They could lead to a contribution of the order of 0.1 on the mean charged-particle multiplicity.

Charged-particle multiplicity analysis

Figures 3 and 4 show the charged-particle multiplicity distribution assuming stable K^0_s and Λ and that including K^0_s and Λ decay products, respectively. Both distributions agree quite well with JETSET and ARIADNE, but HERWIG [20] overestimates the data for low and for high multiplicities.

The high statistics at the Z mass allows us to measure with high accuracy the principal moments of the charged-particle multiplicity, including the skewness S and the kurtosis K. They are summarized in table 1 with and without charged particles resulting from K^0 and Λ decay. The mean charged-particle multiplicity including the decay products of K^0 and Λ is $\langle N_{ch}^{K^0} \rangle = 20.46 \pm 0.01 \pm 0.10$. This result is lower than the previous L3 measurement [24] ($< N_{ch}^{K^0} >= 20.79 \pm 0.03 \pm 0.52$), but agrees within the error.

The higher-order moments H_q are shown in figs. 5 and 6 for the charged-particle multiplicity distributions without and with K^0 and Λ decay products, respectively. Both have a first negative minimum near $q = 5$ and $q = 6$ and both have quasi-oscillations around 0 for higher q. For a stable calculation of the H_q, the multiplicity distributions with and without charged particles resulting from K^0 and Λ decay were truncated at $N_{ch} = 50$ and at $N_{ch} = 48$, respectively. (multiplicities larger than 50 or 48 were removed)

The H_q calculated from JETSET agree quite well with the data in both cases, when the multiplicity distributions are truncated in the same way as the data. The H_q calculated from HERWIG show oscillations with maxima and minima at the same values of q as for the data, but with amplitudes which are much larger.

Charged-particle multiplicities for tagged events

Since analytical pQCD calculations assume massless quarks, and do not take into account mass effects or the weak decay of heavy quarks, a measurement of the H_q moments of the charged-particle multiplicity distribution for only light-quark events allows a better comparison with pQCD calculations. On the other hand using only b-quark events will give the possibility to quantify the influence of the weak decay of heavy quarks on the charged-particle multiplicity distribution.

In order to discriminate between light- and heavy-quark events, we make use of the full 3-dimensional information on tracks from the central tracking detector in order to compute the probability that a track comes from the primary vertex [25]. From these track probabilities, an event discriminant D, on which the selection or rejection of b-quark events is based, is calculated. The distribution of this discriminant is shown in figs. 7 and 8 for the 1994 and 1995 data taking period respectively, for both the data and JETSET for all events, together with the JETSET discriminant distributions for light-quark events (including u,d,s,c-quark contributions) and for b-quark events.

The purity and efficiency of the light-quark event sample, selected by $D < D_{cut}$ are shown in Figs. 9a and 10a as a function of D_{cut} for 1994 and 1995 data samples respectively.

The purity and efficiency of the b-quark event sample, selected by $D > D_{cut}$ are shown in Figs. 9b and 10b as a function of D_{cut} for 1994 and 1995 data samples respectively.

For this analysis, the tagged light-quark event sample was selected by requiring $D < 1.2$. The purity and efficiency of the light-quark sample were for 1994, 93.4% and 89.2%, respectively, and for 1995 93.0% and 91.6%. The tagged b-quark event sample was selected using a $D > 3.4$,

which led to a purity and efficiency in b-quarks for 1994 of 95.2% and 38.8%, respectively, and for 1995 of 97.0% and 37.1%.

The same selection and correction procedures as used on the undifferentiated events were applied to the tagged charged-particle multiplicity distributions. Furthermore, an additional correction factor, $C^{\rm fl}_{\rm purity}(n)$ was applied bin by bin to the tagged charged-particle multiplicity distributions $P^{\rm fl-tagged}_{\rm data}(n)$ to correct the light- and b-quark tagged samples for b- and light-quark contaminations, respectively:

$$P^{\rm fl}_{\rm data}(n) = C^{\rm fl}_{\rm purity}(n) \times P^{\rm fl-tagged}_{\rm data}(n),$$

$$\text{where } C^{\rm fl}_{\rm purity}(n) = P^{\rm fl}_{\rm MC}(n)/P^{\rm fl-tagged}_{\rm MC}(n) \text{ and fl, the flavour of the sample .}$$

The reconstructed charged-particle multiplicity distributions for light and b quarks are shown in fig. 11, together with the untagged charged-particle multiplicity distribution.

JETSET shows an overall good agreement with the light- and b-quark samples (figs. 12 and 13), while HERWIG, as for the untagged charged-particle multiplicity distribution, overestimates high multiplicities for the light- and b-quark samples. (The disagreement is greater for the b-quark sample.)

As for the untagged charged-particle multiplicity distributions, we measured the moments. They are summarized in tables 2 and 3 for the light-quark and b-quark event samples respectively.

The mean charged-particle multiplicity including the decay products of $\rm K^0$ and Λ is found to be $\langle N^{\rm K^0}_{\rm ch}\rangle = 19.88 \pm 0.01 \pm 0.12$ for light-quark events and $\langle N^{\rm K^0}_{\rm ch}\rangle = 22.48 \pm 0.03 \pm 0.18$ for b-quark events. As a check we find that $(1-R_b)\times\langle N^{\rm light}_{\rm ch}\rangle + R_b \times \langle N^{\rm b}_{\rm ch}\rangle$ where $R_b = \sigma(\rm e^+e^- \longrightarrow b\bar{b})/\sigma(e^+e^- \longrightarrow q\bar{q})$, is consistent with the value of $\langle N_{\rm ch}\rangle$ obtained above from the entire sample.

The H_q moments measured for the light- and b-quark charged-particle multiplicity distributions are shown together with those for the untagged one in fig. 14. The H_q moments of the light-quark sample agree very well with those measured for the untagged sample. The H_q moments of the b-quark sample agree within the errors for most of the q, but there is a slight difference for values of q smaller than 5. However, the main difference between the light-quark, b-quark and untagged samples seems to come from the mean itself. For higher moments differences vanish rapidly and have almost disappeared for H_5 and higher q.

Inclusive charged-particle spectrum ξ

We performed a study of the inclusive charged-particle spectrum $\xi = -\ln(2p/\sqrt{s})$ for all, light and b-quark event samples. The ξ distributions were corrected using a procedure similar to the one used for the charged-particle multiplicity distribution:

1. correction for detector acceptance and inefficiencies using the unfolding method described in a previous section. This time the matrix associates the ξ value of a particle to the one of its corresponding detected track. This matrix, taking intrinsically into account of the mis-measurement of track momenta, allows a better reconstruction of the distribution than a simple bin by bin correction especially for high values of ξ. We also added a "0 particle" bin to the matrix in order to treat properly detected tracks lacking of particle (split tracks, remaining bad tracks, ...). This bin acts by rejecting on a statistical basis a certain amount of tracks in each bin.

2. corrections for selection procedure, initial state radiation, light or b-quark contamination, K^0_s and Λ decay products (contrary to how we treated them for the charged-particle multiplicity distribution correction) were performed using a bin by bin procedure.

The statistical errors were estimated assuming Gaussian distributed errors for the data and all terms used to correct the data. Same contributions as for the charged particle multiplicity distribution (described in a previous section) were used for the evaluation of the systematics errors.

The corrected ξ distributions for all, light and b-quark events are shown together with JETSET, which do not describe the data, in fig 15, the errors shown on the plot take into account both statistical and systematic components.

Analytical QCD calculation predicts in the Double Leading Logarithm Approximation (DLLA), assuming LPHD, that the ξ distribution is Gaussian. With next to leading order corrections, the Modified Leading Logarithm Approximation (MLLA) skews and flattens this Gaussian shape [26], shifting the peak value of the ξ spectrum, $\xi^\star$, to a higher value.

We performed fits to the ξ spectrum between 2.4 and 4.8 for all, light and b-quark events using both a Gaussian and the "Fong-Webber" skewed Gaussian [27] which reproduces the shape expected by MLLA around the peak value. The fitted distributions are shown in figures 16, 17, 18 with both Gaussian and skewed Gaussian fit.

The fit of the skewed Gaussian is rather good for the light-quark event sample with $\chi^2 = 24$ for 13 degrees of freedom, which is better than the Gaussian fit, which has $\chi^2 = 30$ for 13 degrees of freedom (fig. 16) For the b-quark event sample the best fit is obtained for the Gaussian with a $\chi^2 = 23$ for 13 degrees of freedom, while the skewed Gaussian fits poorly with $\chi^2 = 96$ for 13 degrees of freedom (fig. 17). This could be explained by the fact that some particles come from the b-quark decay rather than the partonic cascade, effectively diluting the coherence effect.

For the full sample, both the skewed Gaussian and the "normal" Gaussian give poor fits with χ^2 of 38 and 22 for 13 degrees of freedom (confidence level $3 \cdot 10^{-4}$ and $3.1 \cdot 10^{-2}$), respectively. (fig. 18)

We extracted from the fit of the skewed Gaussian the measurement of the peak value $\xi^\star$ for light-quark event and all event samples. For the b-quark event sample, since the Gaussian fit is clearly better, the $\xi^\star$ is measured from the fit by the Gaussian. For the systematic errors we took the same contribution we used for the other measurement to which we added contributions coming from the change in the fit range, we also took into account the fit by the Gaussian instead of the skewed Gaussian for the light-quark event and the all event samples and the fit by the skewed Gaussian instead of a Gaussian for the b-quark event sample, which corresponds to the largest contribution. We found for the ξ distributions where K^0_s and Λ have decayed:

$$\xi^\star_{\rm light} = 3.772 \pm 0.005 \pm 0.022$$
$$\xi^\star_{\rm b} = 3.614 \pm 0.005 \pm 0.045$$
$$\xi^\star_{\rm all} = 3.743 \pm 0.005 \pm 0.029$$

By integrating the ξ spectrum one can obtain a measurement of the mean charged-particle multiplicity. This provides a cross-check of our direct measurement. We found for the ξ distributions where K^0_s and Λ have decayed:

$$\langle N^{\rm light}_{\rm ch} \rangle = 19.93 \pm 0.13 ({\rm stat.} + {\rm syst.})$$

$$\langle N_{\rm ch}^{\rm b} \rangle = 22.53 \pm 0.15(\text{stat.} + \text{syst.})$$
$$\langle N_{\rm ch}^{\rm all} \rangle = 20.48 \pm 0.13(\text{stat.} + \text{syst.})$$

These results are in good agreement with our direct measurements.

Jet multiplicity analysis

Since the behavior of the H_q agrees qualitatively with that predicted in NNLLA, it is natural to interpret this agreement as a confirmation of the NNLLA prediction, and SLD [4] indeed gave this interpretation. However, JETSET agrees with the data, while the parton-shower modeling of JETSET is not at the NNLLA order of pQCD. Hence, the H_q from JETSET should not be expected to oscillate. That it does, together with doubt about the LPHD assumption, suggests that we view the NNLLA interpretation with scepticism.

The jet analysis assumes that the jet multiplicity distribution is related to the parton multiplicity distribution at the energy scale corresponding to the jet resolution. By choosing a scale where perturbative QCD should be applicable ($\gtrsim 1$ GeV), we should be able to test the pQCD predictions for the behavior of the H_q without assuming LPHD. We define jets using the Cambridge jet algorithm [28]. This algorithm uses $y_{ij} = \frac{2\min(E_i^2, E_j^2)}{E_{\rm vis}^2}(1 - \cos\theta_{ij})$ as the distance between particles i and j and combines them by calculating the sum of their momenta (E-scheme).

This algorithm has the property of minimizing hadronization effects, since it can associate particles with large angles and small transverse energies which is a specific effect of hadronization. Furthermore the algorithm allows better treatment of the soft jets by removing them from calculation before any extra particles are associated with them, which leads to a better energy identification of gluon jets than Durham [29].

It has been shown [13–16] in previous analyses of hadronic Z decays (see for review [30]) that mean jet multiplicities agree well with the NLLA prediction in the perturbative region, i.e., for values of $y_{\rm cut}$ greater than 10^{-3}, which corresponds to transverse energies greater than ~ 1 GeV.

Since this study starts with the charged-particle multiplicity distribution, we have also constructed jets using only charged tracks. The charged-particle and jet multiplicities are, of course, identical for sufficiently small values of $y_{\rm cut}$ ($y_{\rm cut} \lesssim 10^{-8}$).

Using both charged and neutral particles instead of only the charged particles gives similar results. We have checked that the fractions of 2-jet and 3-jet events are comparable for $y_{\rm cut} = 0.01$, *i.e.* 63% and 32% for charged and neutral particles and 61% and 32.5% for charged tracks only.

The H_q measured from jet multiplicity distributions have been corrected using the same procedure as for the charged-particle multiplicity distribution (*i.e.* the jets replacing in all corrections terms the charged-particles)

The resulting H_q are shown in figs. 19 and 20, for four different values of $y_{\rm cut}$, representing both non-perturbative and perturbative regions.

A first minimum at $q = 4$ followed by quasi-oscillation about 0 is seen for $y_{\rm cut} = 6.8 \cdot 10^{-6}$ (energy scale $\approx$ 230 MeV) (fig. 19a). This behavior is qualitatively similar to that for the charged-particle multiplicity distribution but both the position of the first minimum and of subsequent maxima and minima are shifted to lower values of q. The same is true for jet multiplicity distributions with smaller $y_{\rm cut}$.

For $y = 1 \cdot 10^{-5}$ (energy scale $\approx$ 290 MeV) the behavior looks similar, except that the first minimum appears at $q = 2$ (see insert in fig. 19b).

For $y_{\rm cut} > 1.5 \cdot 10^{-5}$ and in particular in the perturbative region $y_{\rm cut} \geqslant 10^{-4}$ (corresponding to an energy scale $\gtrsim$ 1 GeV), the negative first minimum near 5 has completely disappeared, as seen in fig. 20 for $y_{\rm cut} \approx 1.2 \cdot 10^{-4}$ (energy scale $\approx$ 1 GeV) and $y_{\rm cut} \approx 8.7 \cdot 10^{-4}$ (energy scale $\approx$ 2.7 GeV). Instead, H_q alternates between positive and negative values for each consecutive q, with an amplitude much larger than that of the oscillation in fig. 19.

None of the predictions made for the H_q at different orders of pQCD is observed. Even though pQCD describes the average jet multiplicity well, it seems to be unable to describe the shape of these distributions. In ref. [31] using the H_q measured from charged-particle multiplicity distributions obtained for restricted rapidity intervals, we have seen that the typical H_q behavior remains even though very low multiplicity distributions are reached. (essentially the first minimum near $q = 5$, since for very low multiplicity distribution it does not make much sense to calculate the H_q for q where the oscillations usually occur). Therefore the disappearance of this behavior for jets is not merely a consequence of the low jet multiplicity. Therefore, the minimum and oscillatory behavior of the H_q seen for the charged-particle multiplicity distribution and for very low values of $y_{\rm cut}$ appears unrelated to the behavior of the H_q calculated in NNLLA.

Monte Carlo study of the oscillatory behavior of the H_q

The H_q calculated from JETSET agree well with the data for each $y_{\rm cut}$, while the H_q calculated from HERWIG disagree in magnitude with the data for low values of $y_{\rm cut}$, where the jet multiplicity distributions are closer to the charged-particle multiplicity distribution.

Given the success of JETSET and HERWIG and the failure of the NNLLA prediction seen in the previous section, we attempted to find that aspect of the Monte Carlo generators which is responsible for the agreement.

We have varied several options in JETSET and studied their influence on the behavior of the H_q. First we used different models of parton generation using in all cases the Lund string fragmentation model. We tried the following:

- no angular ordering in the parton shower, which makes it essentially an LLA shower with the addition of energy-momentum conservation at each branching;
- $\mathcal{O}(\alpha_{\rm s})$ and $\mathcal{O}(\alpha_{\rm s}^2)$ matrix elements instead of a parton shower;
- matrix element production of $\rm q\bar{q}$ only.

Next we considered the possibility that this behavior could come from the fragmentation model, which could simulate some hidden higher-order aspects of pQCD. We used JETSET 7.4 with the various choices of parton generation used previously but with independent fragmentation for the hadronization process. We also used HERWIG 5.9 which uses cluster fragmentation.

In all cases, the H_q have a negative first minimum near $q = 5$ and quasi-oscillations for greater q. Some examples are shown in fig. 21.

This investigation done with Monte Carlo generators shows that an oscillatory behavior of the H_q, reproducing the features (*i.e.* first negative minimum near five and quasi-oscillations) predicted by the NNLLA, can be obtained without the need of the NNLLA of pQCD

Conclusions

The ratio of cumulant factorial to factorial moments, H_q, has been measured for both the charged-particle and jet multiplicity distributions, the latter obtained with the Cambridge jet algorithm. A perturbative QCD calculation at the next-to-next-to-leading logarithm approximation predicts H_q to have a negative first minimum at $q \approx 5$ and quasi-oscillation around 0 for higher q. This behavior is observed for our charged-particle multiplicity distribution, confirming previous results. The same behavior is also observed for the light-quark charged-particle multiplicity distribution, which was also found in good agreement with the total charged-particle multiplicity distribution. For b-quark events, there is a slight difference in H_q for small q, but for $q \geq 5$ there is agreement with the full sample. Thus, the H_q moments don't seem to be very sensitive to quark mass effects. However, our analysis of the H_q of the jet multiplicity distributions reveals that this behavior appears only for very small $y_{\rm cut}$, corresponding to energy scales $\lesssim$ 100 MeV, which is far from the perturbative region. Furthermore, an investigation performed on different models of parton generation and on different fragmentation models has shown oscillatory behavior of H_q in each case.

From this we conclude that the oscillations of H_q observed in the charged-particle multiplicity distribution at the Z mass are unlikely to be related to the behavior predicted by the NNLLA perturbative QCD calculations.

References

[1] E.A. De Wolf, I.M. Dremin, W. Kittel, Phys. Rep. **270** (1996).

[2] I.M. Dremin, Physics-Uspekhi **37** (1994) 715.

[3] I.M. Dremin, Phys. Lett. **B 313** (1993) 209;
I.M. Dremin and V.A. Nechitaĭlo, JETP Lett. **58** (1993) 881.

[4] SLD Collab., K. Abe *et al.*, Phys. Lett. **B 371** (1996) 149.

[5] A. Giovannini, S. Lupia, R. Ugoccioni, Phys. Lett. **B 374** (1996) 231.

[6] R. Ugoccioni, Proc. XXVI Int. Symp. on Multiparticle Dynamics, eds. J. Dias de Deus *et al.*(World Scientific, Singapore, 1997) p.208.

[7] Aleph Collab.,D. Buskulic *et al.*, Z. Phys **C 69** (1995) 15.

[8] Delphi Collab., P. Abreu *et al.*, Z. Phys. **C 52** (1991) 271.

[9] Opal Collab., B. Acton *et al.*, Z. phys. **C 53** (1992) 539.

[10] N. Nakajima, M. Biyajima and N. Suzuki, Phys. Rev. **D 54** (1996) 4333;
Wang Shaoshun *et al.*, Phys. Rev. **D 56** (1997) 1668;
A. Capella *et al.*, Z. Phys. **C 75** (1997) 89;
I.M. Dremin *et al.*, Phys. Lett. **B 403** (1997) 149.

[11] DELPHI Collab., P. Abreu *et al.*, Nucl. Phys. **B 1** (1995) 3.

[12] OPAL Collaboration, R. Akers *et al.*, Z. Phys. **C 68** (1995) 1.

[13] OPAL Collab., R. Akers *et al.*, Z. Phys. **C 63** (1994) 363.

[14] L3 Collab., O. Adriani *et al.*, Phys. Rep. **236** (1993) 1.

[15] A. Buytenhuijs, QCD gluon radiation studies using the L3 detector, Ph.D. thesis, University of Nijmegen, 1996, The Netherlands, http://www.hef.kun.nl/publ/publ-phd-theses/buytenhuijs/ps/thesis.ps.gz .

[16] ALEPH Collab., R. Barate *et al.*, Phys. Rep. **294** (1998) 1.

[17] L3 Collab., B. Adeva *et al.*, Nucl. Instr. Meth. **A 289** (1990) 35;
J.A. Bakken *et al.*, Nucl. Instr. Meth. **A 275** (1989) 81;
O. Adriani *et al.*, Nucl. Instr. Meth. **A 302** (1991) 53;
B. Adeva *et al.*, Nucl. Instr. Meth. **A 323** (1992) 109;
K. Deiters *et al.*, Nucl. Instr. Meth. **A 323** (1992) 162;
B. Acciari *et al.*, Nucl. Instr. Meth. **A 351** (1994) 300;
A. Adam *et al.*, Nucl. Instr. Meth. **A 383** (1996) 342.

[18] T. Sjöstrand, Comp. Phys. Comm. **39** (1986) 347;
T. Sjöstrand and M. Bengtsson, Comp. Phys. Comm. **43** (1987) 367..

[19] U. Pettersson, LU TP 88-5 (1988)
L. Lönnblad, LU TP 91-11 (1991) .

[20] G. Marchesini and B. Webber, Nucl. Phys. **B 310** (1988) 461;
G. Marchesini *et al.*, Comp. Phys. Comm. **67** (1992) 465..

[21] S. Banerjee, D. Duchesneau, S. Sarkar, L3 Note 1818 (1995);
J. Casaus, L3 Note 1946 (1996);
L3 Collab., B. Adeva *et al.*, Z. Phys. **C 55** (1992) 39.

[22] The L3 detector simulation is based on GEANT, see R. Brun *et al.*, CERN report CERN DD/EE/84-1 (Revised), 1987, and uses GHEISHA to simulate hadronic interactions, see RWTH Aachen report PITHA 85/02, 1985.

[23] G. Susinno, L3 Note 1996 (1996).

[24] L3 Collab., B. Adeva *et al.*, Z. Phys. **C55** (1992) 39.

[25] J.G. Branson, A. Dominguez, I. Fisk, G. Raven, L3 Note 2108 (1997);
L3 Collab., M. Acciarri *et al.*, Phys. Lett. **B 411** (1997) 373;
A. Dominguez, Ph.D. thesis, University of California at San Diego (1998).
http://hep.ucsd.edu/thesis/aaron.html .

[26] Yu.L. Dokshitzer *et al.*, Basics of Perturbative QCD, Editions Frontières, Gif-sur-Yvette, 1991. .

[27] C.P. Fong and B.R. Webber, Phys. Lett. **B229** (1989) 289. .

[28] Yu.L. Dokshitzer, G.D. Leder, S. Moretti, B.R. Webber, JHEP **08** (1997) 001.

[29] S. Bethke, Z. Kunszt, D.E. Soper and W.J. Stirling, Nucl. Phys. **B 370** (1992) 310.

[30] V.A. Khoze and W. Ochs, Perturbative QCD approach to multiparticle production, Preprint MPI-PhT/96-29; Durham DTP/96/36; HEP-PH/97011421, 1996.

[31] D.J. Mangeol, Proc. 8th Int. Workshop on Multiparticle Production, eds. T. Csörgő *et al.*(World Scientific, Singapore, 1999) p.342.

Variable	without K^0 and Λ decay			with K^0 and Λ decay		
	Value	Error		Value	Error	
		Stat.	Syst.		Stat.	Syst.
$\langle N_{\rm ch} \rangle$	18.63	$\pm$ 0.01	$\pm$ 0.10	20.46	$\pm$ 0.01	$\pm$ 0.10
$\langle N_{\rm ch}^2 \rangle$	381.7	$\pm$ 0.3	$\pm$ 4.2	457.7	$\pm$ 0.3	$\pm$ 4.6
$\langle N_{\rm ch}^3 \rangle$	8524	$\pm$ 10	$\pm$ 148	11108	$\pm$ 12	$\pm$ 176
$\langle N_{\rm ch}^4 \rangle$	205878	$\pm$ 357	$\pm$ 4960	290548	$\pm$ 470	$\pm$ 6406
$\mathcal{D} = \sqrt{\langle (N_{\rm ch} - \langle N_{\rm ch} \rangle)^2 \rangle}$	5.886	$\pm$ 0.005	$\pm$ 0.051	6.244	$\pm$ 0.005	$\pm$ 0.050
$\langle N_{\rm ch} \rangle / \mathcal{D}$	3.165	$\pm$ 0.002	$\pm$ 0.016	3.278	$\pm$ 0.002	$\pm$ 0.015
$S = \langle (N_{\rm ch} - \langle N_{\rm ch} \rangle)^3 \rangle / \mathcal{D}^3$	0.596	$\pm$ 0.003	$\pm$ 0.010	0.600	$\pm$ 0.003	$\pm$ 0.008
$K = \langle (N_{\rm ch} - \langle N_{\rm ch} \rangle)^4 \rangle / \mathcal{D}^4 - 3$	0.51	$\pm$ 0.01	$\pm$ 0.04	0.49	$\pm$ 0.01	$\pm$ 0.03

Table 1: Moments of the charged-particle multiplicity distribution for all events

Variable	without K^0 and Λ decay			with K^0 and Λ decay		
	Value	Error		Value	Error	
		Stat.	Syst.		Stat.	Syst.
$\langle N_{\rm ch} \rangle$	18.07	$\pm$ 0.01	$\pm$ 0.09	19.88	$\pm$ 0.01	$\pm$ 0.09
$\langle N_{\rm ch}^2 \rangle$	360.0	$\pm$ 0.3	$\pm$ 3.9	432.4	$\pm$ 0.4	$\pm$ 4.3
$\langle N_{\rm ch}^3 \rangle$	7827	$\pm$ 11	$\pm$ 134	10220	$\pm$ 14	$\pm$ 160
$\langle N_{\rm ch}^4 \rangle$	184370	$\pm$ 390	$\pm$ 4458	260701	$\pm$ 531	$\pm$ 5730
$\mathcal{D} = \sqrt{\langle (N_{\rm ch} - \langle N_{\rm ch} \rangle)^2 \rangle}$	5.769	$\pm$ 0.007	$\pm$ 0.053	6.111	$\pm$ 0.007	$\pm$ 0.052
$\langle N_{\rm ch} \rangle / \mathcal{D}$	3.133	$\pm$ 0.003	$\pm$ 0.019	3.252	$\pm$ 0.003	$\pm$ 0.017
$S = \langle (N_{\rm ch} - \langle N_{\rm ch} \rangle)^3 \rangle / \mathcal{D}^3$	0.613	$\pm$ 0.005	$\pm$ 0.013	0.617	$\pm$ 0.005	$\pm$ 0.011
$K = \langle (N_{\rm ch} - \langle N_{\rm ch} \rangle)^4 \rangle / \mathcal{D}^4 - 3$	0.54	$\pm$ 0.02	$\pm$ 0.06	0.53	$\pm$ 0.02	$\pm$ 0.05

Table 2: Moments of the charged-particle multiplicity distribution for udsc-quark events

Variable	without K^0 and Λ decay			with K^0 and Λ decay		
	Value	Error		Value	Error	
		Stat.	Syst.		Stat.	Syst.
$\langle N_{\rm ch} \rangle$	20.51	$\pm$ 0.03	$\pm$ 0.13	22.45	$\pm$ 0.03	$\pm$ 0.13
$\langle N_{\rm ch}^2 \rangle$	454	$\pm$ 1	$\pm$ 6	542	$\pm$ 1	$\pm$ 6
$\langle N_{\rm ch}^3 \rangle$	10787	$\pm$ 40	$\pm$ 208	14006	$\pm$ 48	$\pm$ 249
$\langle N_{\rm ch}^4 \rangle$	273891	$\pm$ 1457	$\pm$ 7148	385758	$\pm$ 1883	$\pm$ 9284
$\mathcal{D} = \sqrt{\langle (N_{\rm ch} - \langle N_{\rm ch} \rangle)^2 \rangle}$	5.78	$\pm$ 0.01	$\pm$ 0.05	6.16	$\pm$ 0.01	$\pm$ 0.05
$\langle N_{\rm ch} \rangle / \mathcal{D}$	3.551	$\pm$ 0.006	$\pm$ 0.010	3.645	$\pm$ 0.005	$\pm$ 0.009
$S = \langle (N_{\rm ch} - \langle N_{\rm ch} \rangle)^3 \rangle / \mathcal{D}^3$	0.574	$\pm$ 0.017	$\pm$ 0.007	0.573	$\pm$ 0.017	$\pm$ 0.006
$K = \langle (N_{\rm ch} - \langle N_{\rm ch} \rangle)^4 \rangle / \mathcal{D}^4 - 3$	0.43	$\pm$ 0.04	$\pm$ 0.03	0.42	$\pm$ 0.04	$\pm$ 0.03

Table 3: Moments of the charged-particle multiplicity distribution for b-quark events

List of Figures

1 Factorial moments F_q and ratio of cumulant to factorial moment H_q as a function of their moment rank for a Poisson distribution and for a Negative Binomial Distribution.

2 Predictions at different order of perturbative QCD for the H_q as a function the moment rank q.

3 Comparison of the charged-particle multiplicity distribution without K^0 and Λ decay products with JETSET and HERWIG. Errors include both statistical and systematics contributions.

4 Comparison of the charged-particle multiplicity distribution with K^0 and Λ decay products added with JETSET and HERWIG. Errors include both statistical and systematics contributions.

5 Comparison of the H_q measured from the charged-particle multiplicity distribution with stable K^0 and Λ with JETSET and HERWIG. The errors shown include both statistical and systematic contributions.

6 H_q of the of the charged-particle multiplicity distribution including K^0 and Λ decay products with JETSET and HERWIG. Errors include both statistical and systematics contributions.

7 Event discriminant distribution for the 1994 data compared with the discriminant distributions of the Monte Carlo for all events, b quarks events and light quarks events.

8 Event discriminant distribution for the 1995 data compared with the discriminant distributions of the Monte Carlo for all events, b quarks events and light quarks events.

9 The efficiency and purity of the light-quark sample (a) as a function of the cut on the discriminant value selecting light quarks ($D < D_{\rm cut}$), and the efficiency and purity in b quarks (b) as a function of a cut on the discriminant value selecting b-quark sample ($D > D_{\rm cut}$) for the year 1994

10 The efficiency and purity of the light-quark sample (a) as a function of the cut on the discriminant value selecting light quarks ($D < D_{\rm cut}$), and the efficiency and purity in b quarks (b) as a function of a cut on the discriminant value selecting b-quark sample ($D > D_{\rm cut}$) for the year 1995

11 The charged-particle multiplicity distribution including K^0 and Λ decay products of the data for light and b-quark events compared to the one for all events

12 The charged-particle multiplicity distribution including K^0 and Λ decay products for light-quark events together with the ones of JETSET 7.4 PS and HERWIG 5.9

13 The charged-particle multiplicity distribution including K^0 and Λ decay products for b-quark events together with the ones of JETSET 7.4 PS and HERWIG 5.9

14 The H_q measured from the charged-particle multiplicity distribution, including K^0 and Λ decay products for tagged light-quarks and b-quark events compared to the ones measured for JETSET 7.4, together with the H_q moments measured from the charged-particle multiplicity distribution for all events

15 charged-particle momentum spectra ξ for light-quark, b-quark and all event samples together with JETSET expectations for the three samples

16 ξ distribution plotted with gaussian and skewed gaussian fits for light-quark event sample

17 ξ distribution plotted with gaussian and skewed gaussian fits for b-quark event sample

18 ξ distribution plotted with gaussian and skewed gaussian fits for all events

19 H_q of the jet multiplicity distributions obtained with the Cambridge jet algorithm at non-perturbative energy scales, (a) for $y_{\text{cut}} = 6.8 \cdot 10^{-6}$, (b) for $y_{\text{cut}} = 1 \cdot 10^{-5}$.

20 H_q of the jet multiplicity distributions obtained with the Cambridge jet algorithm at perturbative energy scales, (a) for $y_{\text{cut}} = 1.2 \cdot 10^{-4}$, (b) for $y_{\text{cut}} = 8.7 \cdot 10^{-4}$.

21 H_q for the charged-particle multiplicity distribution obtained from Monte Carlo generators using different methods of parton generation and different models of fragmentation.

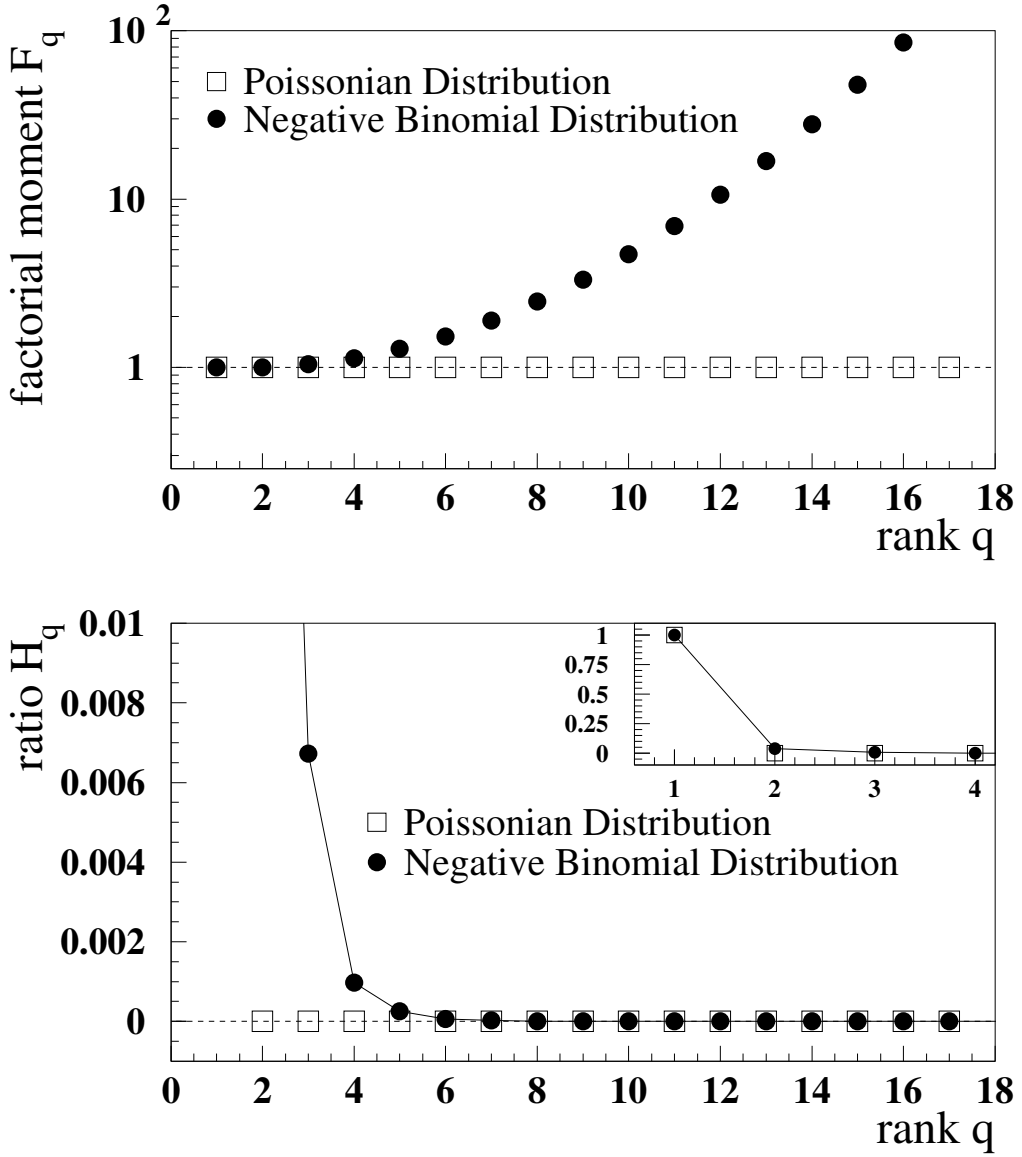

Figure 1: Factorial moments F_q and ratio of cumulant to factorial moment H_q as a function of their moment rank for a Poisson distribution and for a Negative Binomial Distribution.

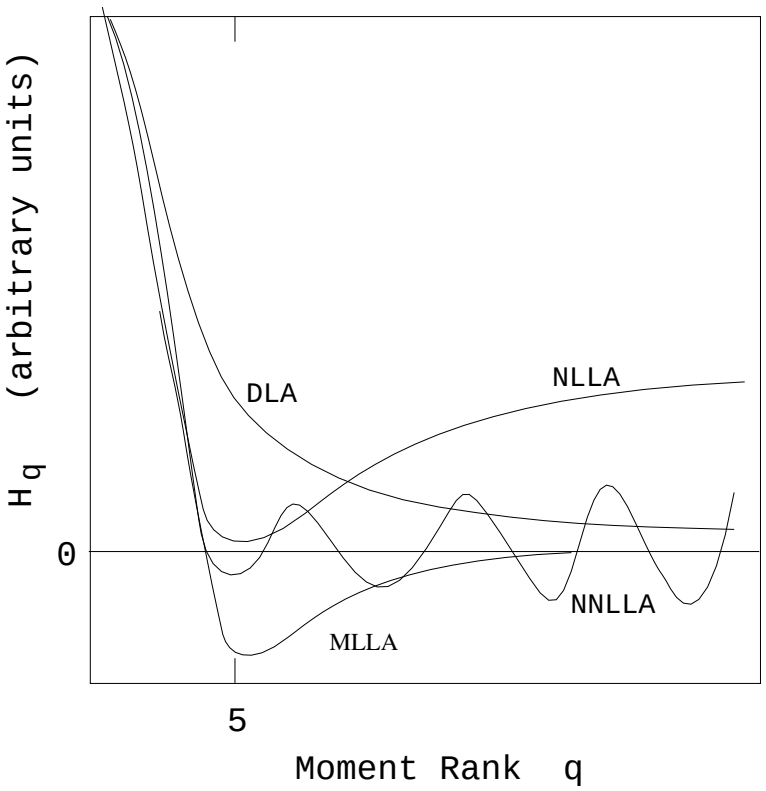

Figure 2: Predictions at different order of perturbative QCD for the H_q as a function the moment rank q.

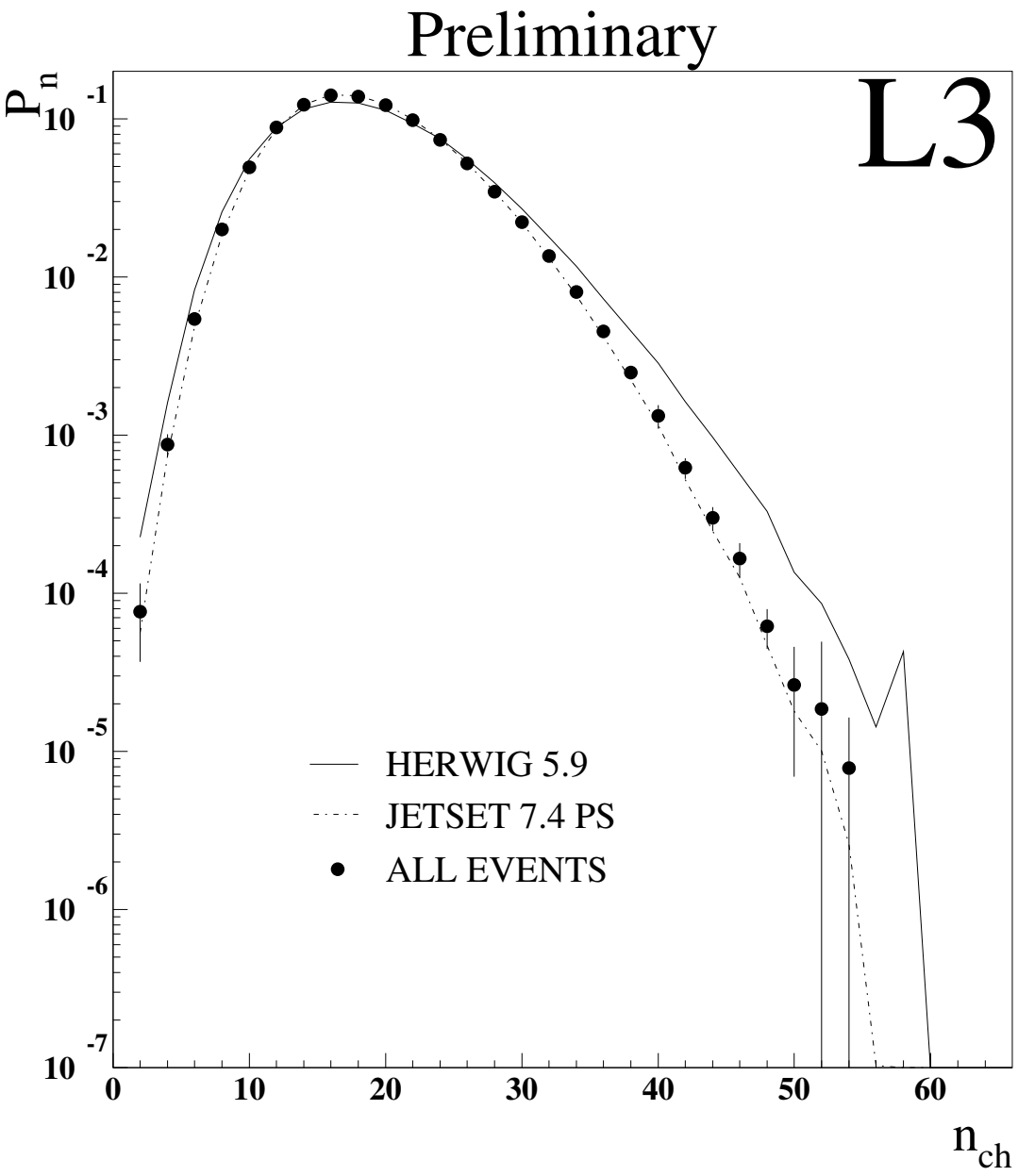

Figure 3: Comparison of the charged-particle multiplicity distribution without K^0 and Λ decay products with JETSET and HERWIG. Errors include both statistical and systematics contributions.

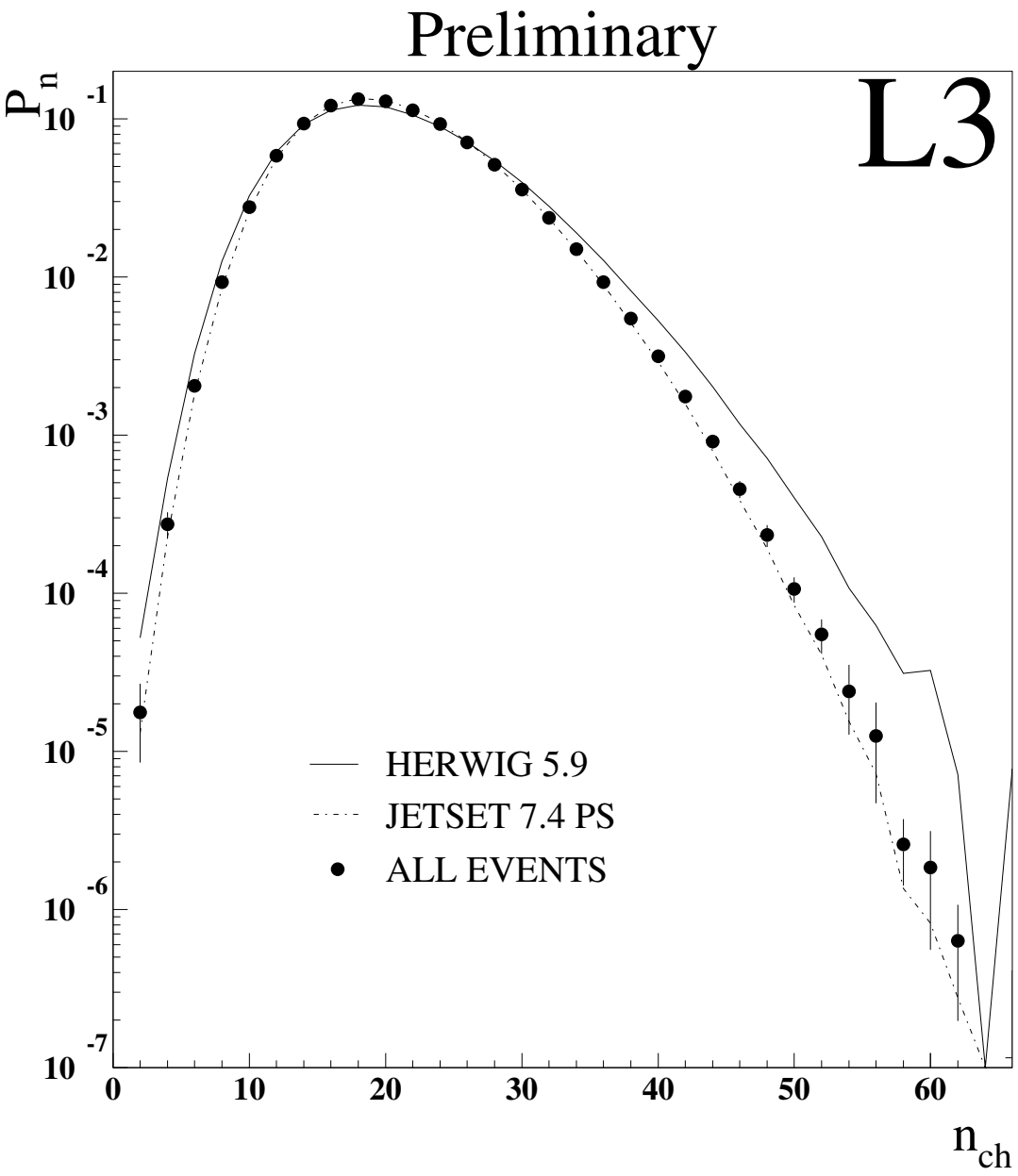

Figure 4: Comparison of the charged-particle multiplicity distribution with K^0 and Λ decay products added with JETSET and HERWIG. Errors include both statistical and systematics contributions.

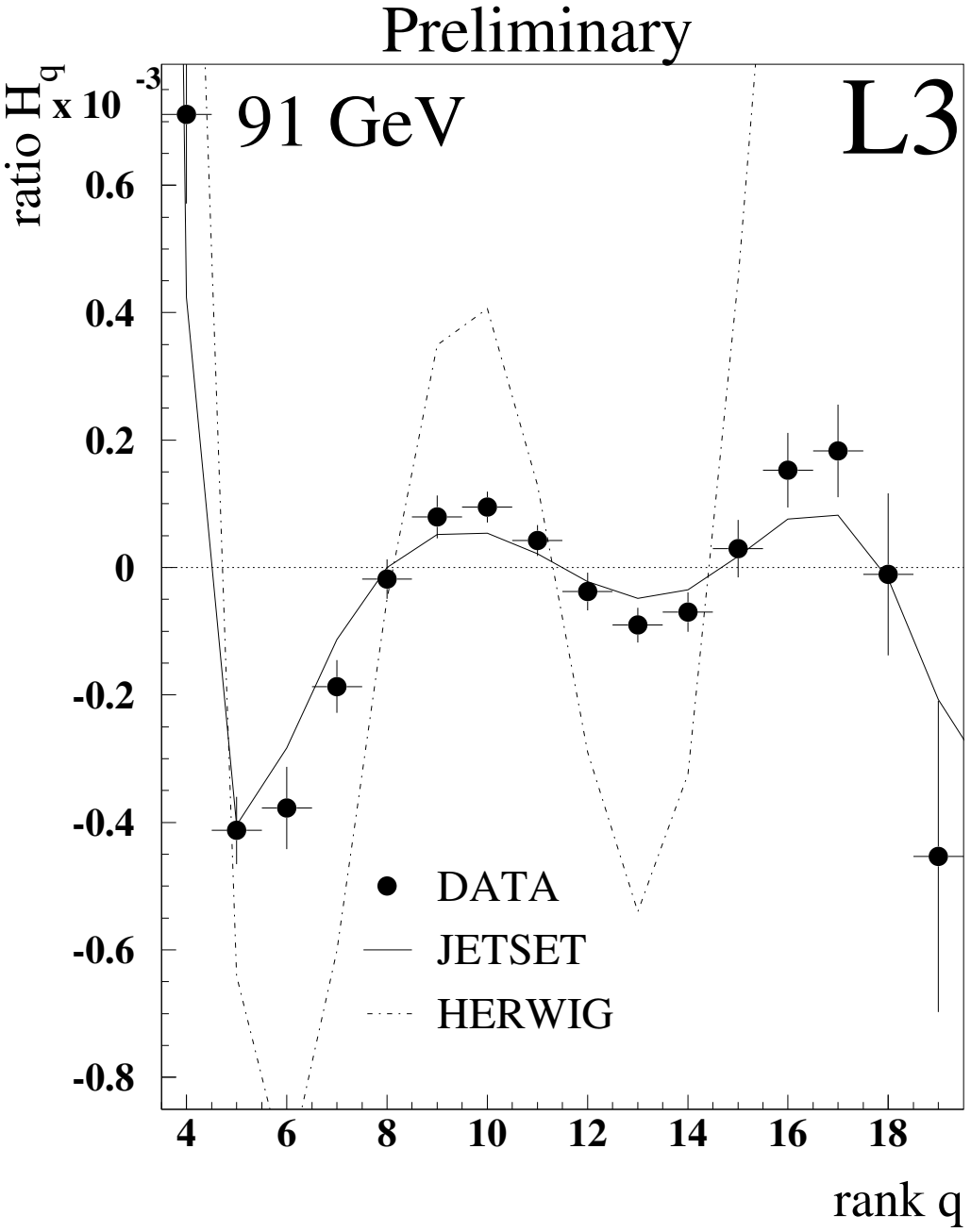

Figure 5: Comparison of the H_q measured from the charged-particle multiplicity distribution with stable K^0 and Λ with JETSET and HERWIG. The errors shown include both statistical and systematic contributions.

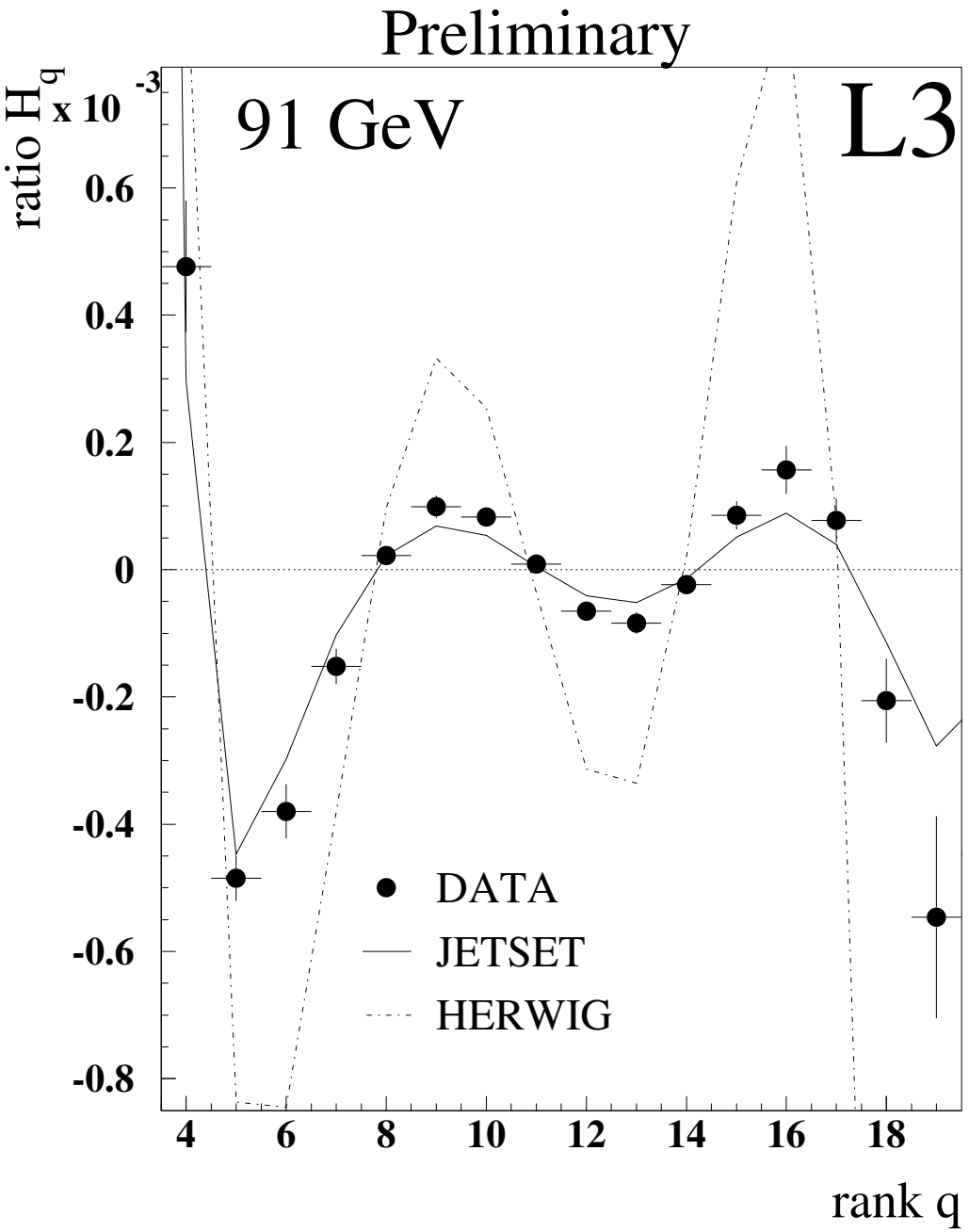

Figure 6: H_q of the of the charged-particle multiplicity distribution including K^0 and Λ decay products with JETSET and HERWIG. Errors include both statistical and systematics contributions.

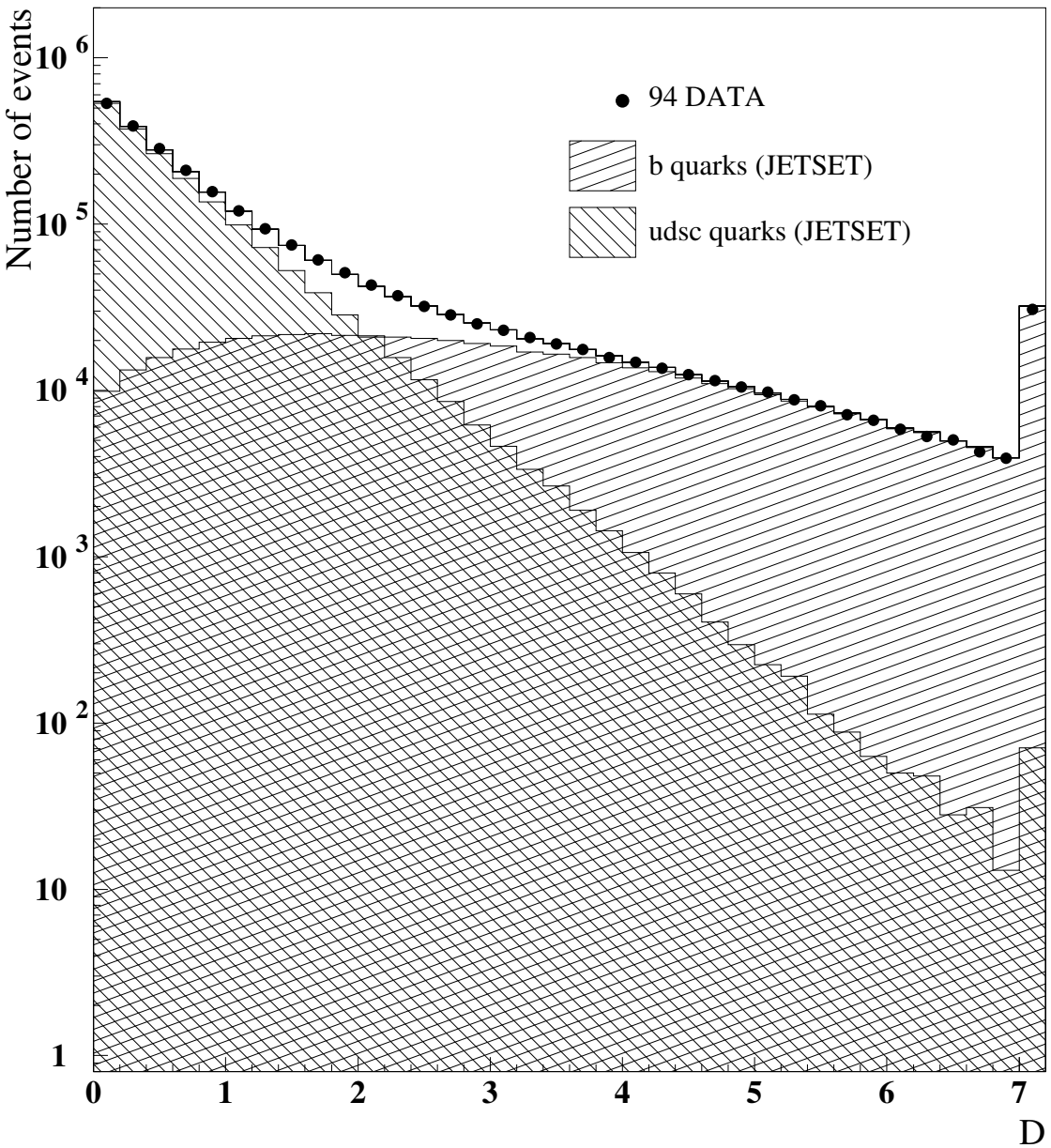

Figure 7: Event discriminant distribution for the 1994 data compared with the discriminant distributions of the Monte Carlo for all events, b quarks events and light quarks events.

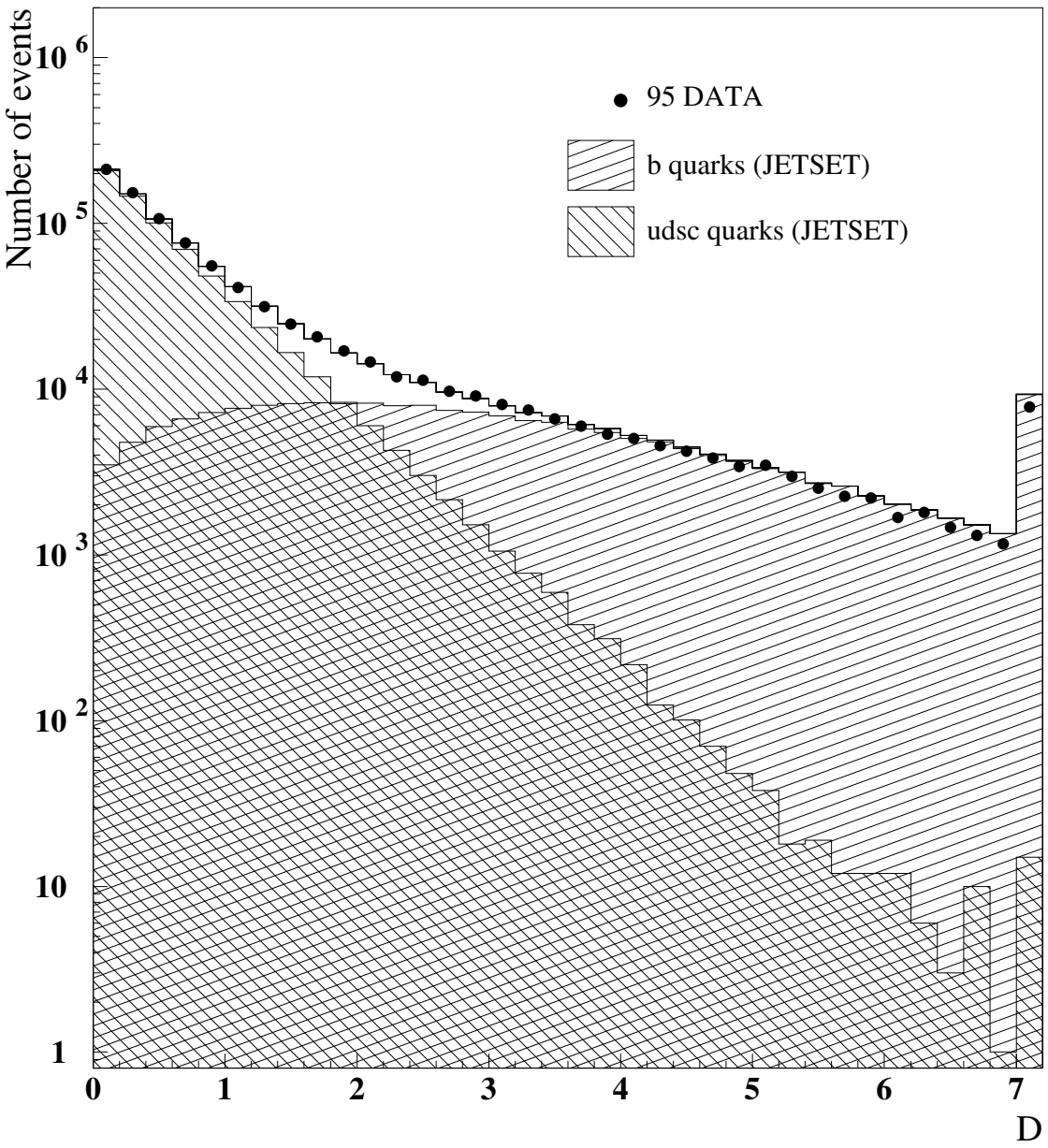

Figure 8: Event discriminant distribution for the 1995 data compared with the discriminant distributions of the Monte Carlo for all events, b quarks events and light quarks events.

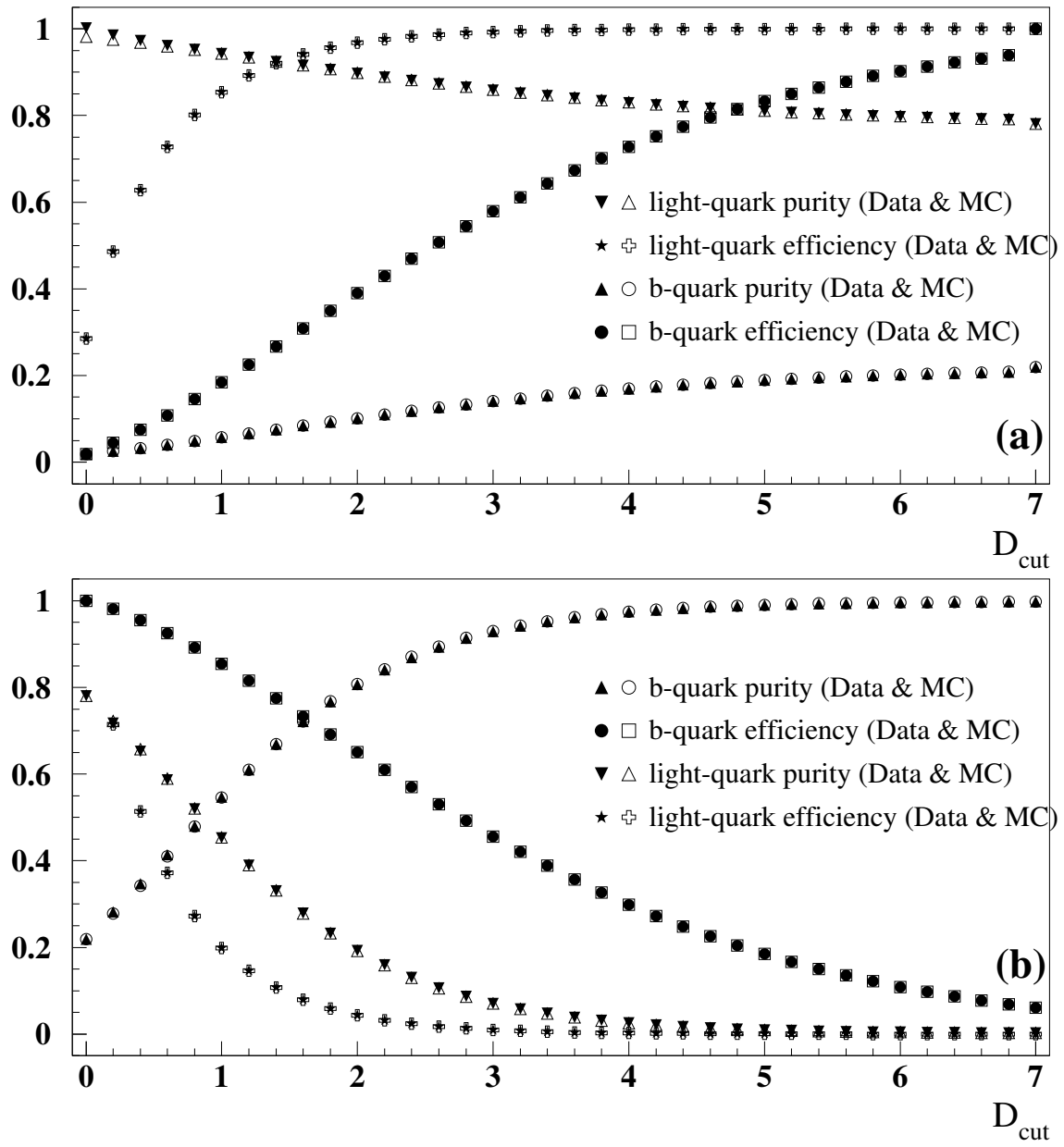

Figure 9: The efficiency and purity of the light-quark sample (a) as a function of the cut on the discriminant value selecting light quarks ($D < D_{\rm cut}$), and the efficiency and purity in b quarks (b) as a function of a cut on the discriminant value selecting b-quark sample ($D > D_{\rm cut}$) for the year 1994

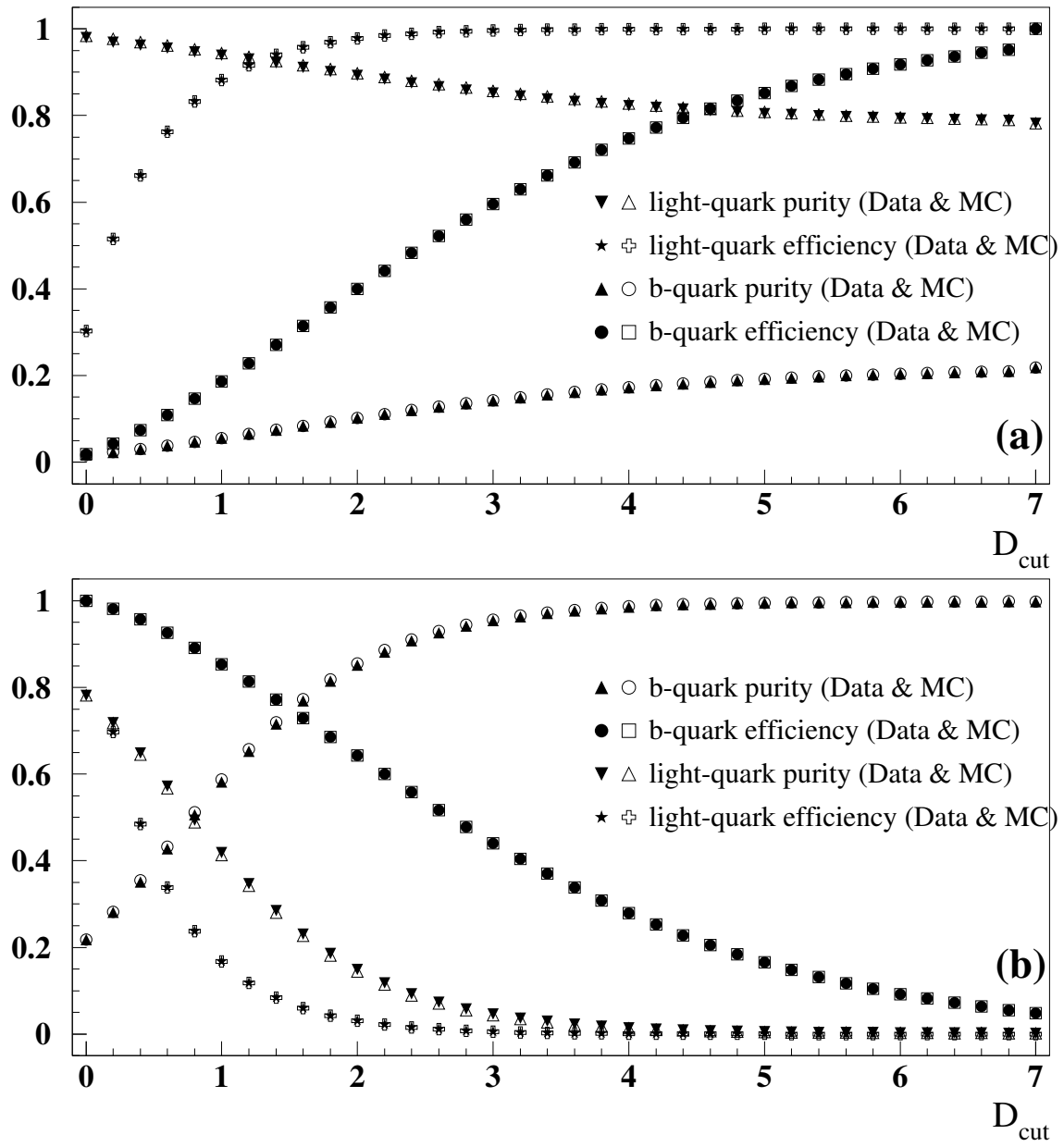

Figure 10: The efficiency and purity of the light-quark sample (a) as a function of the cut on the discriminant value selecting light quarks ($D < D_{\rm cut}$), and the efficiency and purity in b quarks (b) as a function of a cut on the discriminant value selecting b-quark sample ($D > D_{\rm cut}$) for the year 1995

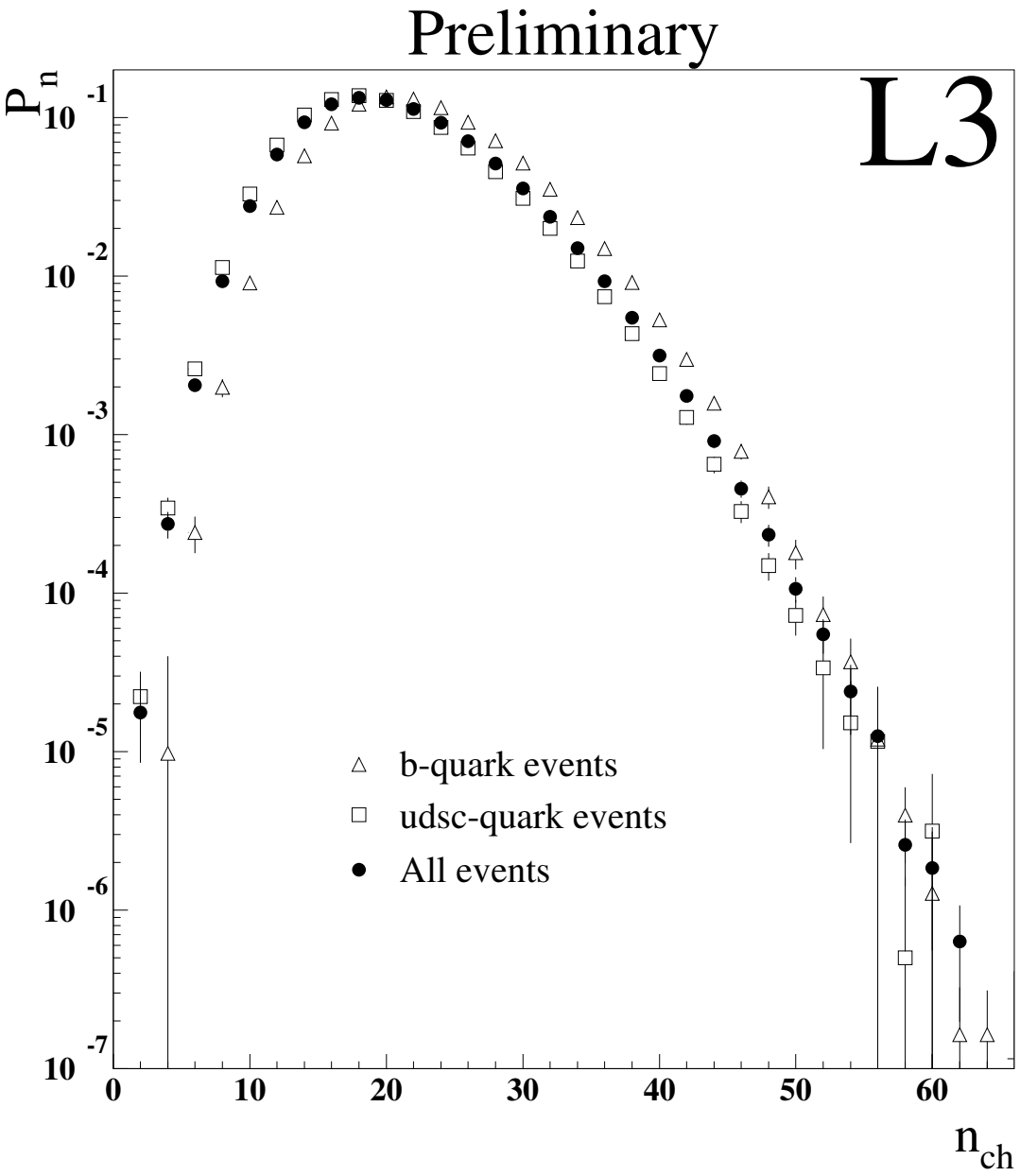

Figure 11: The charged-particle multiplicity distribution including K^0 and Λ decay products of the data for light and b-quark events compared to the one for all events

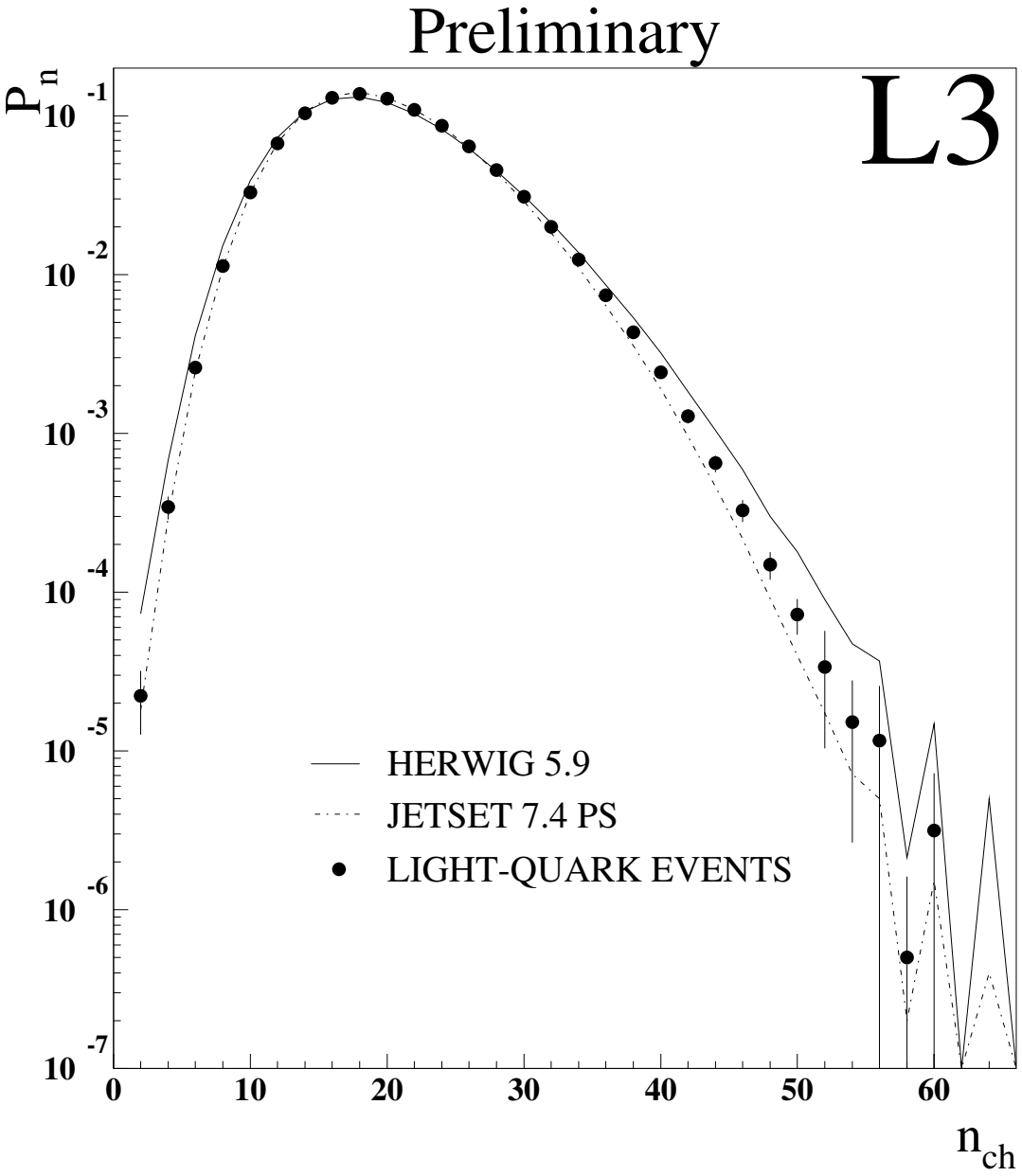

Figure 12: The charged-particle multiplicity distribution including K^0 and Λ decay products for light-quark events together with the ones of JETSET 7.4 PS and HERWIG 5.9

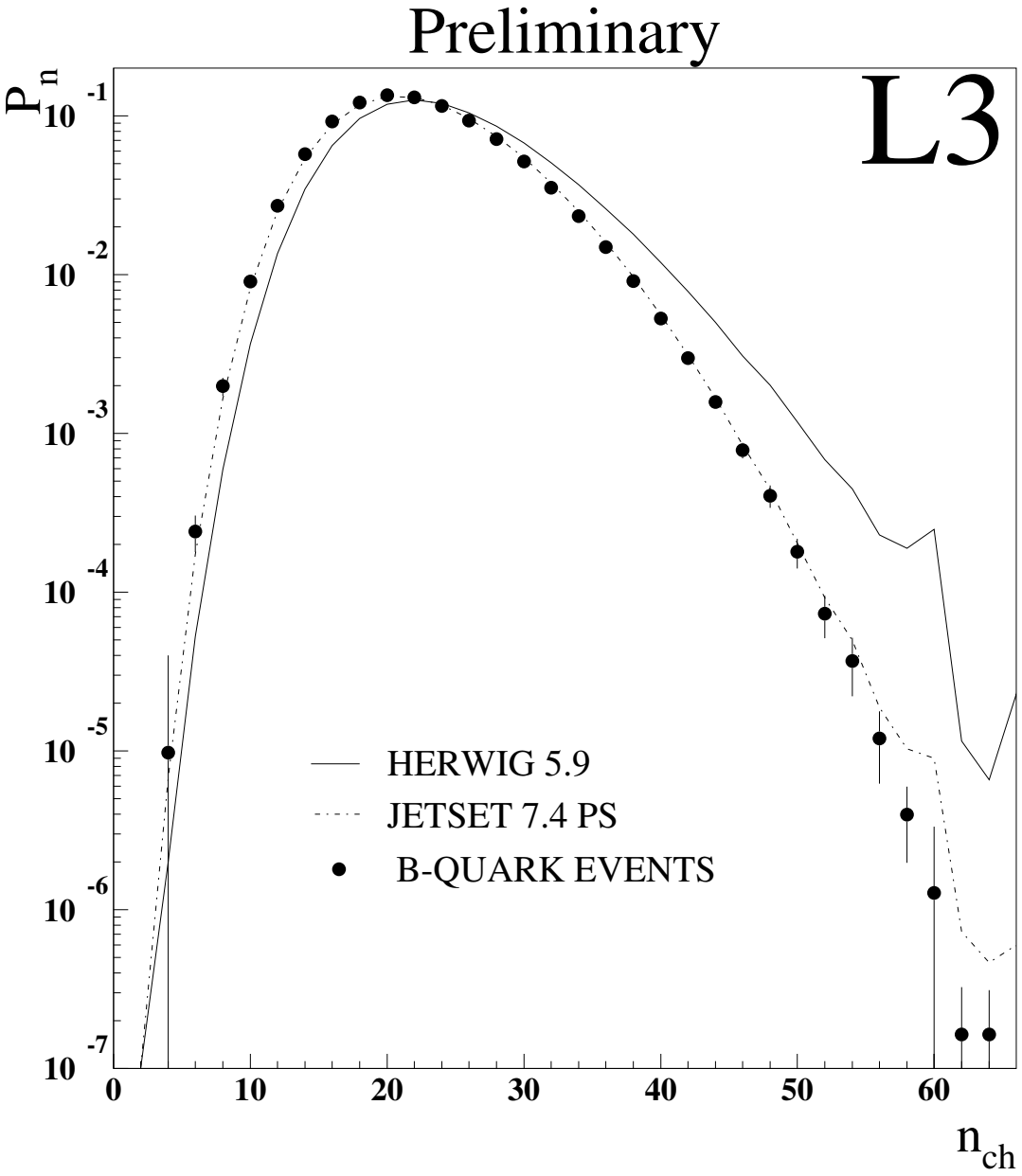

Figure 13: The charged-particle multiplicity distribution including K^0 and Λ decay products for b-quark events together with the ones of JETSET 7.4 PS and HERWIG 5.9

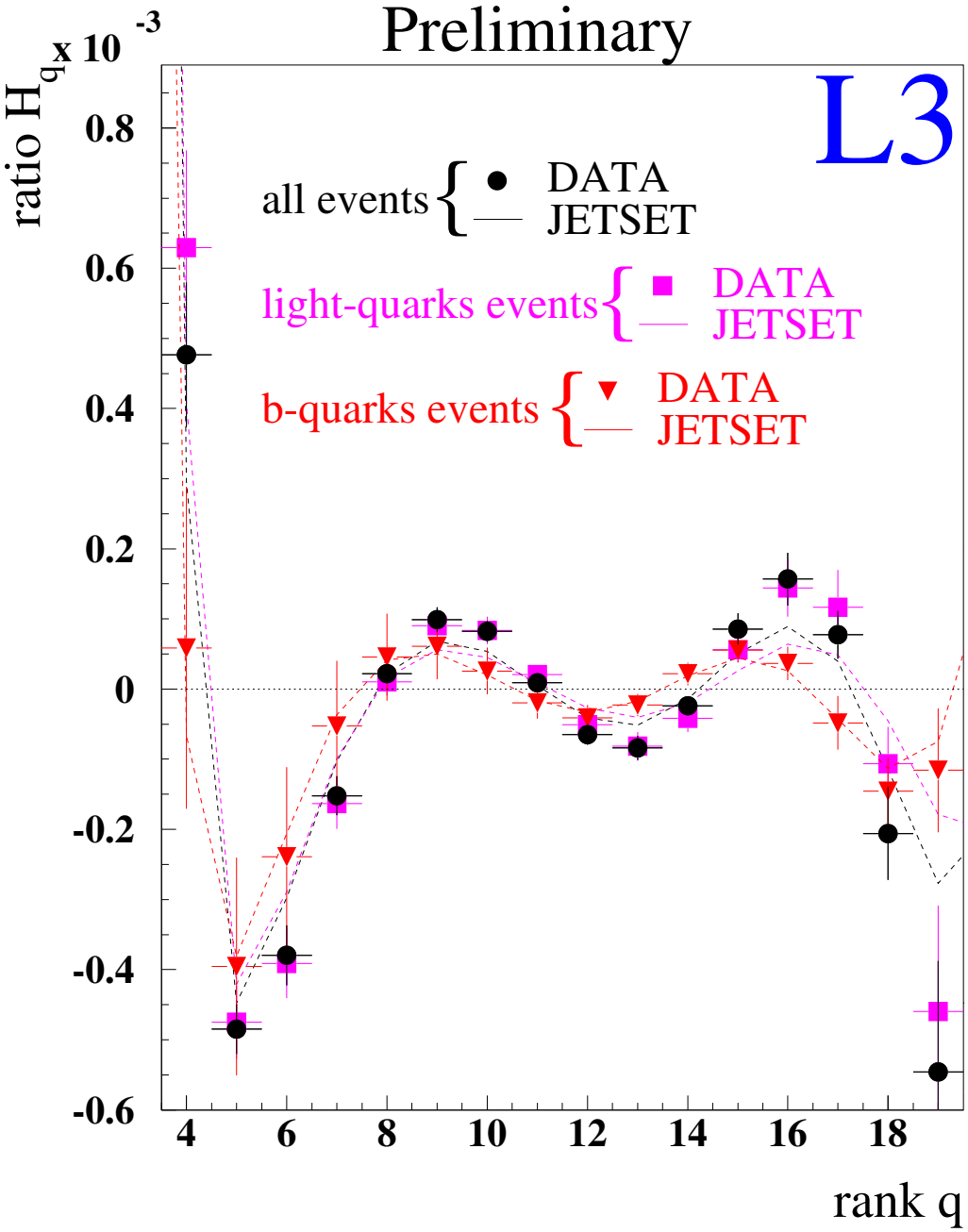

Figure 14: The H_q measured from the charged-particle multiplicity distribution, including K^0 and Λ decay products for tagged light-quarks and b-quark events compared to the ones measured for JETSET 7.4, together with the H_q moments measured from the charged-particle multiplicity distribution for all events

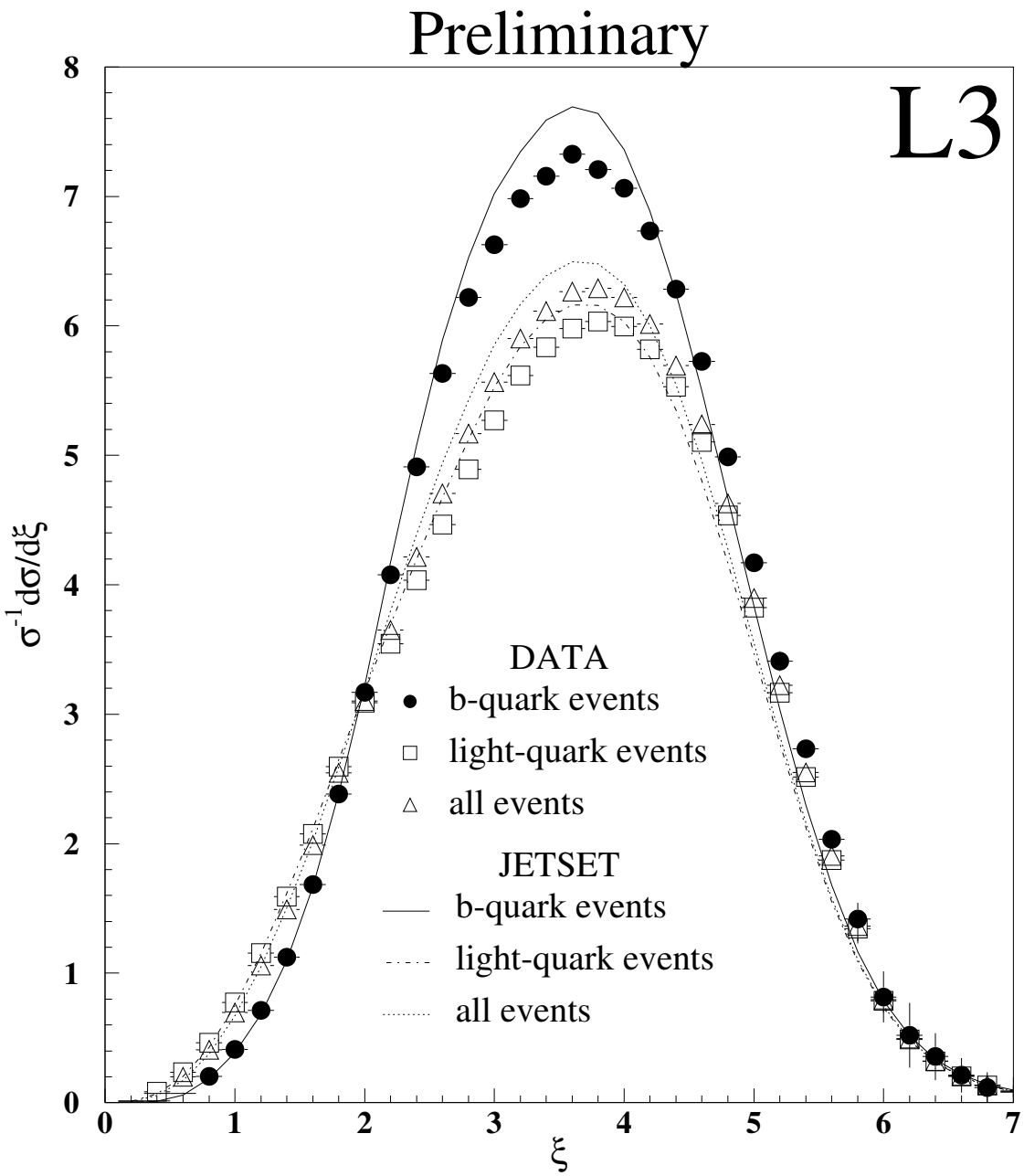

Figure 15: charged-particle momentum spectra ξ for light-quark, b-quark and all event samples together with JETSET expectations for the three samples

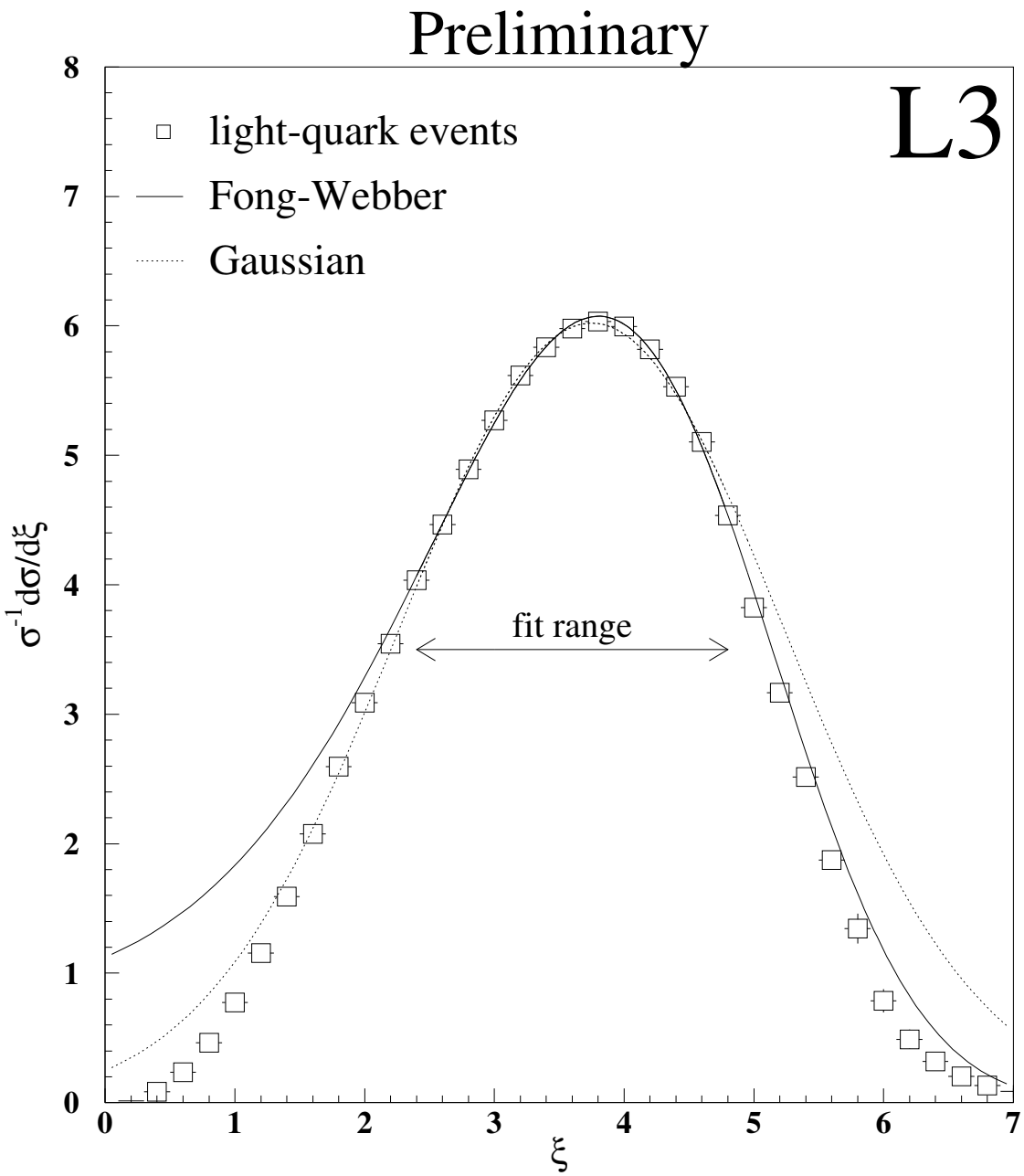

Figure 16: ξ distribution plotted with Gaussian and skewed Gaussian fits for light-quark event sample

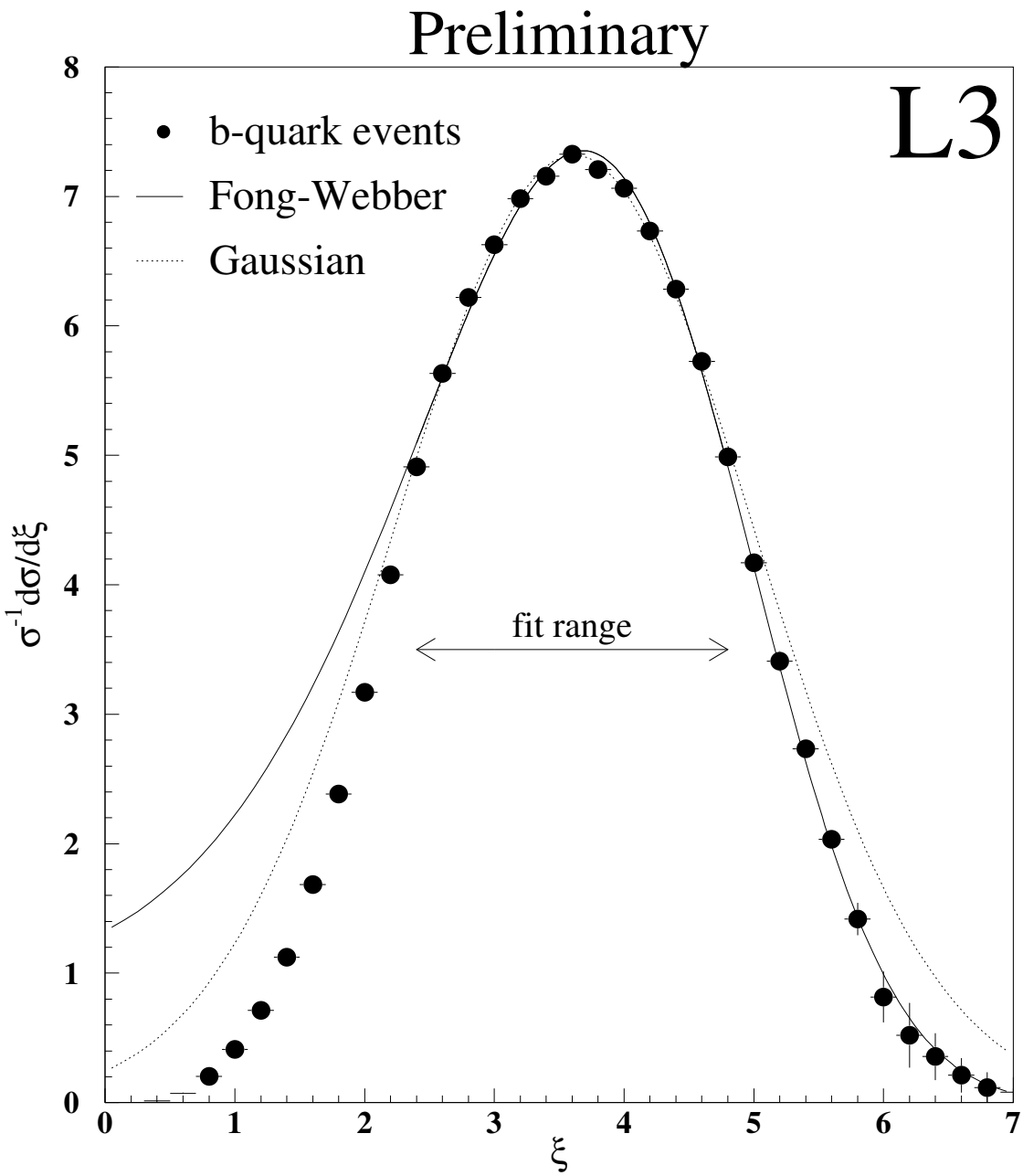

Figure 17: ξ distribution plotted with Gaussian and skewed Gaussian fits for b-quark event sample

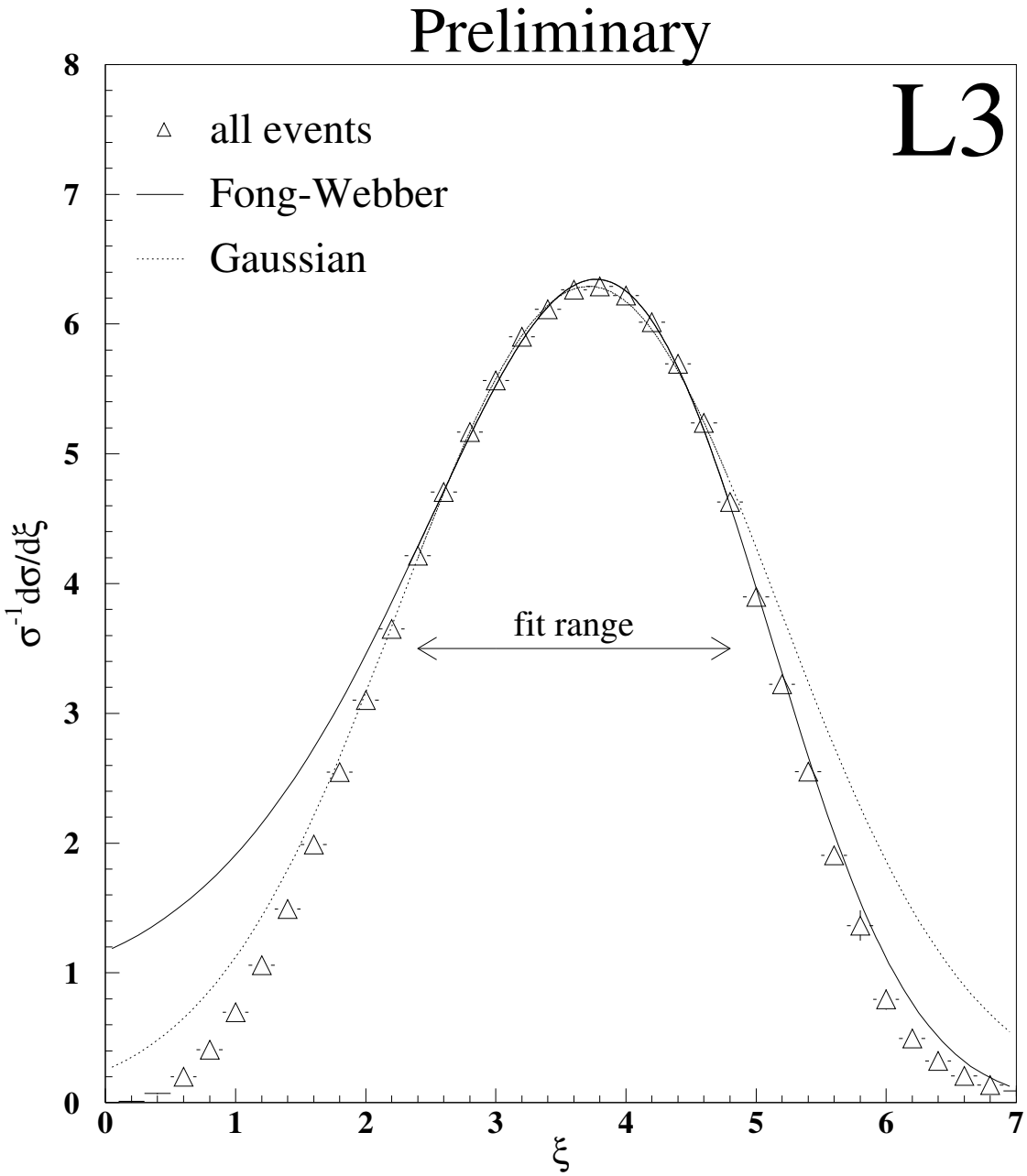

Figure 18: ξ distribution plotted with Gaussian and skewed Gaussian fits for all events

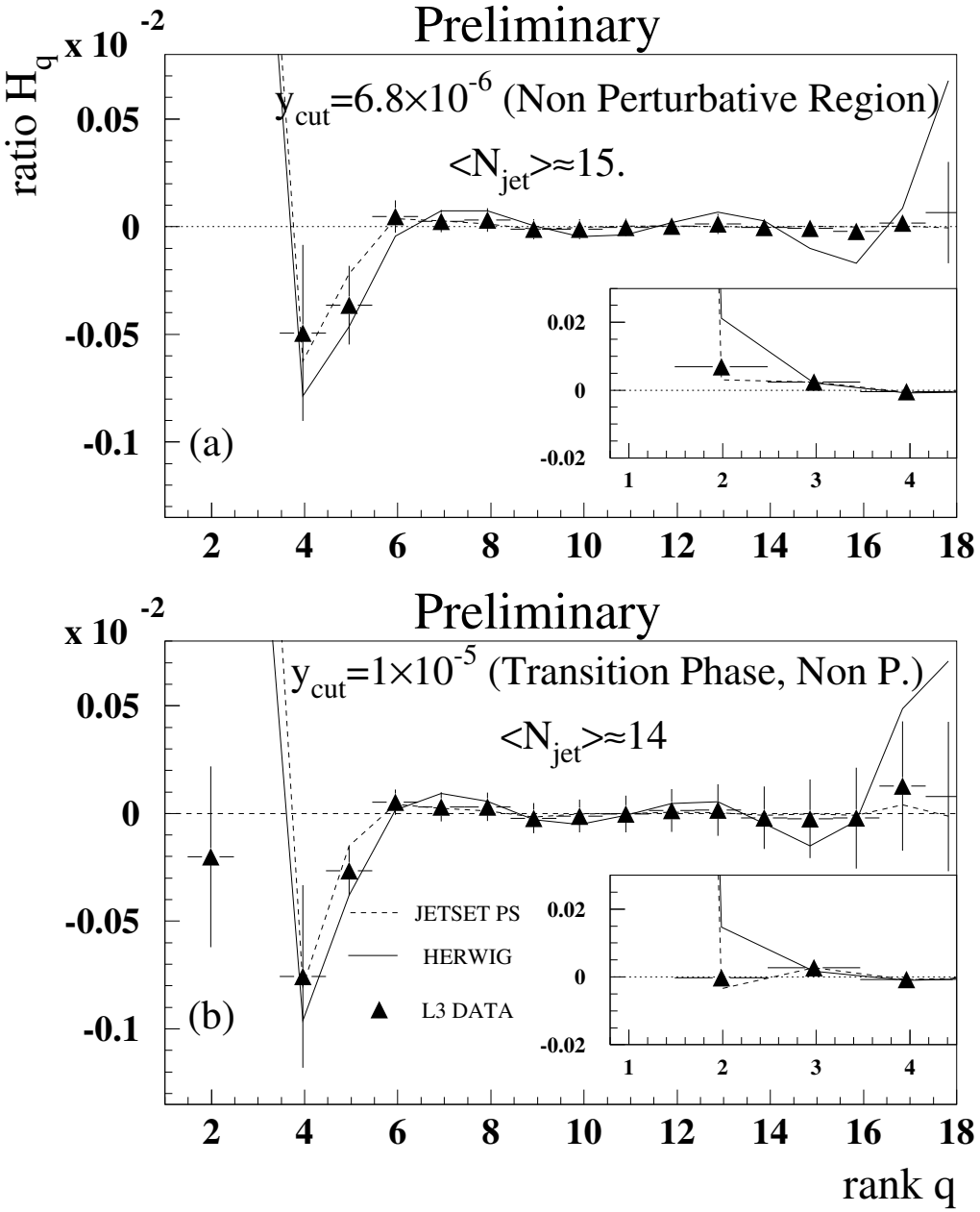

Figure 19: H_q of the jet multiplicity distributions obtained with the Cambridge jet algorithm at non-perturbative energy scales, (a) for $y_{\rm cut} = 6.8 \cdot 10^{-6}$, (b) for $y_{\rm cut} = 1 \cdot 10^{-5}$.

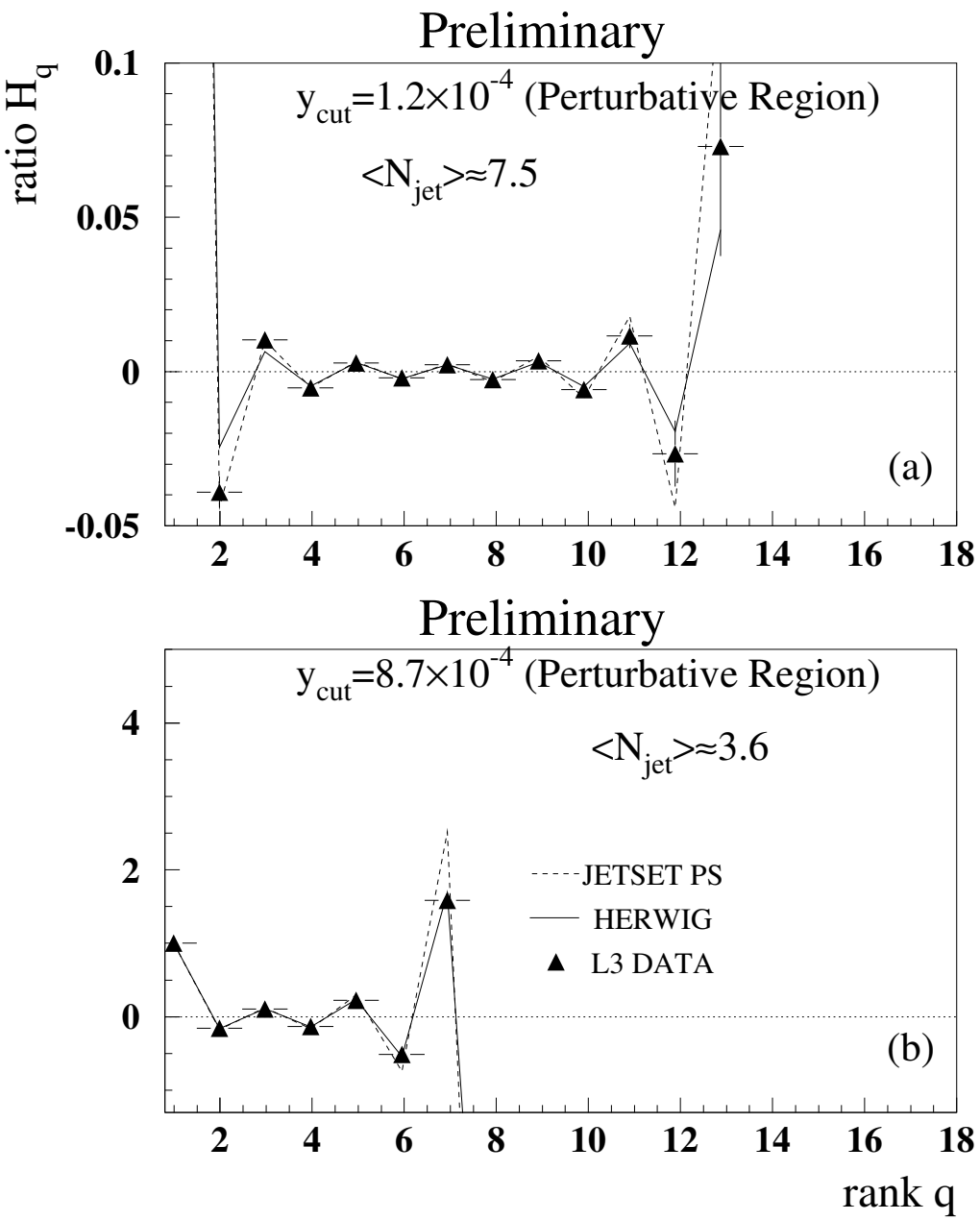

Figure 20: H_q of the jet multiplicity distributions obtained with the Cambridge jet algorithm at perturbative energy scales, (a) for $y_{\rm cut} = 1.2 \cdot 10^{-4}$, (b) for $y_{\rm cut} = 8.7 \cdot 10^{-4}$.

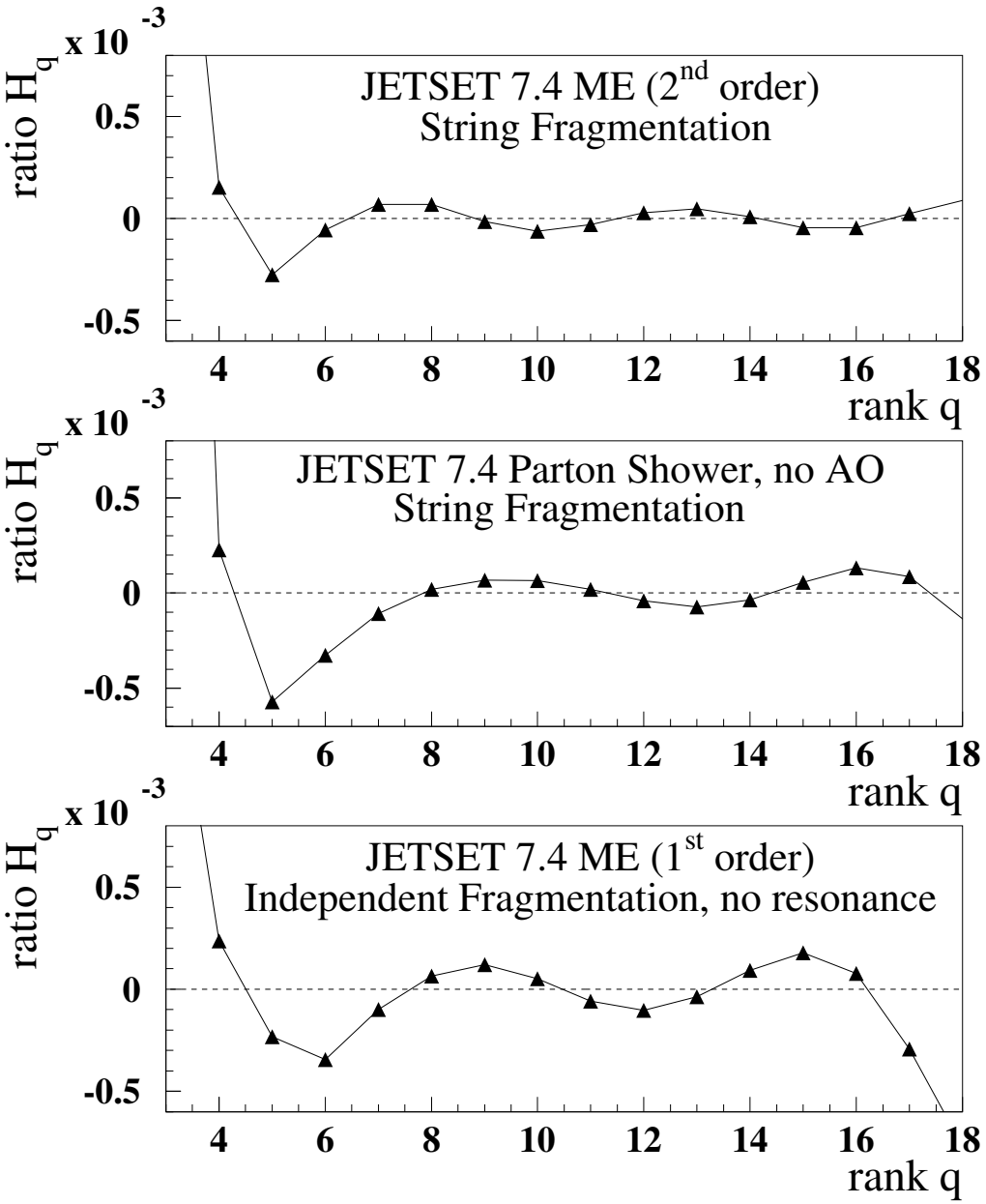

Figure 21: H_q for the charged-particle multiplicity distribution obtained from Monte Carlo generators using different methods of parton generation and different models of fragmentation.